

Survey of O VI absorption in the Large Magellanic Cloud

A. Pathak^{*}, A. C. Pradhan, N. V. Sujatha and J. Murthy

Indian Institute of Astrophysics, Koramangala II Block, Bangalore 560034, India

ABSTRACT

We present a survey of interstellar O VI absorption in the Large Magellanic Cloud (LMC) towards 70 lines of sight based on *Far Ultraviolet Spectroscopic Explorer (FUSE)* observations. The survey covers O VI absorption in a large number of objects in different environmental conditions of the LMC. Overall, a high abundance of O VI is present in active and inactive regions of the LMC with mean $\log N(\text{O VI}) = 14.23$ atoms cm^{-2} . There is no correlation observed between O VI absorption and emissions from the hot gas (X-ray surface brightness) or the warm gas ($\text{H}\alpha$ surface brightness). O VI absorption in the LMC is patchy and the properties are similar to that of the Milky Way (MW). In comparison to the Small Magellanic Cloud (SMC), O VI is lower in abundance even though SMC has a lower metallicity compared to the LMC and the MW. We present observations in 10 superbubbles of the LMC of which we detect O VI absorption in 5 superbubbles for the first time and the superbubbles show an excess O VI absorption of about 40% compared to non-superbubble lines of sight. We have also studied the properties of O VI absorption in the 30 Doradus region. Even though O VI does not show any correlation with X-ray emission for the LMC, a good correlation between $\log N(\text{O VI})$ and X-ray surface brightness for 30 Doradus region is present. We also find that O VI abundance decreases with increasing distance from the star cluster R136.

Key words: galaxies: ISM – ISM: structure – ISM: atoms – galaxies: individual: Large Magellanic Cloud – ultraviolet: ISM

1 INTRODUCTION

The interstellar medium (ISM) of the Milky Way (MW) and other galaxies is a complex mix of gas and dust. The processes involved in maintaining the mass, energy, and ionization balance of the ISM are not properly understood. High resolution ultraviolet (*UV*) spectra provides information about these processes as many absorption lines of atoms, ions and molecules are present in the *UV* band of the electromagnetic spectrum, one of the most important of which is O^{+5} (O VI), a diagnostic of temperatures of about 3×10^5 K (Cox 2005). Such temperatures are found at the interface of hot ($T > 10^6$ K) and warm ($T \sim 10^4$ K) ionized gas in the ISM. Thus, O VI absorption lines at 1031.9 Å and 1037.6 Å are crucial diagnostics of the energetic processes of interface environments in the ISM of galaxies. The gas at such temperatures is cooling radiatively and the cooling is essentially independent of density, metallicity and the heating mechanism (Edgar & Chevalier 1986; Heckman et al. 2002). O VI formation by photo-ionization is unable to explain the observed abundances, given the energy of photons needed to get such high ionization (114 eV).

O VI is mostly produced by shock heating and is collisionally ionized (Indebetouw & Shull 2004).

Previous studies of O VI have been limited to observations by the *Copernicus* satellite (Jenkins 1978a,b) and the *Hopkins Ultraviolet Telescope* (Dixon et al. 1996). Shelton & Cox (1994) concluded that the hot gas exists in discrete regions rather than being continuously present in the ISM. The launch of *Far Ultraviolet Spectroscopic Explorer (FUSE)*; (Moos et al. 2000; Sahnou et al. 2000) enabled a wider and more descriptive study of O VI absorption and emission in the ISM and the intergalactic medium (IGM). With a spectral resolution of 20,000, *FUSE* has been able to resolve fine details of O VI in many different environments. *FUSE* observed O VI absorption lines in the local ISM of the MW (Savage et al. 2000; Wakker et al. 2003; Oegerle et al. 2005; Savage & Lehner 2006; Welsh & Lallement 2008), disk of the MW (Bowen et al. 2008), halo of the MW (Savage et al. 2003), the Large Magellanic Cloud (LMC; Howk et al. (2002a); Lehner & Howk (2007)), the Small Magellanic Cloud (SMC; Hoopes et al. (2002)), starburst galaxies (Grimes et al. 2009), IGM (Danforth & Shull 2005; Danforth et al. 2006), etc. Apart from absorption studies, *FUSE* has also recorded O VI spectra in emission from observations of diffuse ISM in the MW (Shelton et al. 2001;

* e-mail: amitp@iiap.res.in; amitpah@gmail.com

Shelton 2002; Dixon et al. 2006; Dixon & Sankrit 2008) and superbubbles in the LMC (Sankrit & Dixon 2007). These studies have not only augmented our knowledge about the formation and distribution of O VI in the MW and the Magellanic Clouds but have also helped in better understanding of the complexities of the ISM.

Owing to the contiguity to the MW (~ 50 kpc; Feast (1999)) and being nearly a face-on galaxy with a low inclination angle ($\sim 35^\circ$; van der Marel & Cioni (2001)), the LMC has been the subject of numerous studies to understand and interpret the properties of ISM. Recent studies of the ISM in the LMC include observations of diffuse UV emission (Cole et al. 1999a,b; Pradhan et al. 2010), the *SPITZER* infrared dust survey (SAGE; Meixner et al. (2006); Bernard et al. (2008)), the HI survey (Kim et al. 2003), the H_α survey (Gaustad et al. 2001), the O VI distribution (Howk et al. 2002a), and the survey of hot gas in the X-ray bands (Snowden & Petre 1994). More recently, Lehner & Howk (2007) analyzed the absorption of O VI, C IV, Si IV and N V ions towards four early type stars in the LMC and provide crucial details about the environments that may be probed through the study of these ions.

Howk et al. (2002a) surveyed the distribution and kinematics of O VI towards 12 early type stars in the LMC, which was very selective and the targets were restricted to Wolf-Rayet stars and O-type stars of spectral types O7 and earlier. Here we report an extensive survey of O VI absorption at 1032 \AA in the LMC. The observation log is given in Table 1. The results presented in this survey become important as they not only provide a detailed mapping of the interface gas traced by O VI but also throw light on the small scale structure of the O VI distribution in various regions of the LMC. Fig. 1 shows the lines of sight and different regions of the LMC including the superbubbles (marked by circles) that have been studied in this survey.

2 OBSERVATIONS AND DATA ANALYSIS

2.1 *FUSE* data analysis and possible contamination

The *FUSE* mission and its operations are described by Moos et al. (2000) and Sahnou et al. (2000). Observations are made through one of 3 apertures: the HIRS ($1.25'' \times 20''$); the MDRS ($4'' \times 20''$); and the LWRS ($30'' \times 30''$), with all three obtaining data simultaneously. Depending on the coating of the spectrograph, observations are possible through SiC and LiF channels that are further divided into eight different segments; the SiC 1A, SiC 2A, SiC 1B and SiC 2B segments covering the wavelength range 905 to 1105 \AA and LiF 1A, LiF 2A, LiF 1B and LiF 2B segments covering the wavelength range 1000 to 1187 \AA . The data from SiC 2B segment have been known to suffer from a fixed noise. The sensitivity of LiF 1A segment near 1032 \AA is almost double that of other segments and therefore, we have used only the LiF 1A observations (Sahnou et al. 2000). Most of the data are from the large aperture LWRS with a few from the MDRS aperture.

The fully calibrated *FUSE* spectra were downloaded from the Multimission Archive at STScI (MAST) processed by the latest *FUSE* data reduction pipeline (CALFUSE version 3.2; Dixon et al. (2007)). *FUSE* made more than 600

pointings in and around the LMC. Several of the observations were rejected initially by just looking at the spectra (with non-existent or low signal-to-noise of O VI absorption). 70 unique *FUSE* targets were selected based mainly on the simplicity of the continuum fitting in the vicinity of O VI (at 1031.9 \AA). O VI absorption for 1 of the sightline has been reported by Friedman et al. (2000), 11 have been covered by Howk et al. (2002a) survey, 3 by Danforth & Blair (2006) and 1 by Lehner & Howk (2007). Spectral types and other stellar information was taken from Danforth et al. (2002) and Blair et al. (2009). We have downgraded all the spectra reported here to 35 km s^{-1} to have a higher signal-to-noise. This has been done for all the spectra irrespective of the quality to maintain uniformity in the data analysis procedure.

Fitting the stellar continuum in the neighbourhood of the O VI absorption profile has been discussed in detail by Friedman et al. (2000) and Howk et al. (2002a). Howk et al. (2002a) have limited their study to early type stars based on the fact that these stars have completely developed O VI P Cygni profiles that are easier to fit as the early type stars have a high mass loss rate and have minimal wind variations. Lehner et al. (2001, 2003) have shown that for Galactic sight lines, the stellar wind variability has negligible effect on O VI absorption but may introduce substantial errors towards targets in the Magellanic clouds. Lehner et al. (2001) did find variation in the equivalent width and column density towards a LMC star when estimated at two different times. This warrants for extra care while fitting the continuum for Magellanic cloud targets.

As discussed above, for the LMC, the estimation of stellar continuum in the vicinity of O VI absorption is not trivial. Our background targets are mostly early O and B type stars with several Wolf-Rayets. These have been selected based on the fact that the the continuum near the O VI absorption at 1031.9 \AA is simple to fit. A few of the lines of sight do show a complex behaviour near O VI absorption (for e.g., Sk-67D05, Sk-67D168, Sk-70D115, etc.). For such exceptional lines of sight, the complexity in the continuum fitting is due to a local dip or a sudden rise near the O VI absorption and these targets needed a comparatively higher order polynomial for the fitting. For a flavour of the complexity involved, sample continuum fitting for three lines of sight, B113, Sk-70D115 and Sk-67D168 are shown in Fig. 2. Following the fitting procedure of Howk et al. (2002a) and Sembach & Savage (1992), the local stellar continuum was estimated for all the targets and were fitted by a Legendre polynomial fit of low order (≤ 5). Several continua were tested and the uncertainties involved for the complete data set were used in the measurement of the O VI column densities. The normalized spectra in the vicinity of O VI absorption are presented in Fig. 3.

The O VI absorption may be contaminated by absorption from molecular hydrogen, however, it is minimal in the LMC velocity range. This is because the molecular fraction of H_2 in the LMC is only about 12% of the molecular fraction in the Galactic disk (Tumlinson et al. 2002). The closest absorption line of H_2 to O VI absorption in the LMC lies at 1032.35 \AA (at $v_{lsr} \sim +123 \text{ km s}^{-1}$), which is due to (6-0) R(4) transition. An estimation of possible contamination by H_2 towards 12 lines of sight in the LMC has been done by Howk et al. (2002a) where they find that H_2 absorption does

not affect the LMC O VI column densities significantly. The H₂ absorption feature are usually not a problem for measurements of O VI absorption at velocities more than 20 km s⁻¹ apart (Savage et al. (2003) and references therein). We estimate the contamination from H₂ lines by fitting the (6-0) P(3) H₂ transition for the MW and (6-0) R(4) H₂ transition for the LMC (Fig. 4). From this, we are able to estimate the contamination due to (6-0) R(4) MW H₂ line and (6-0) P(3) LMC H₂ line. Noticeable contamination is seen for the sightlines Sk-71D45 and Sk-67D250 which is well within the error bar of the derived column densities. An example of a sightline is also shown in Fig. 4 in which the LMC O VI absorption is free from any contamination from molecular hydrogen. Owing to the negligible contribution, we have not excluded the contamination by H₂ in the O VI measurements for the LMC.

Another possible contaminant is the (6-0) R(0) transition of the HD molecule at 1031.91 Å that overlaps with the MW O VI absorption. Several lines of HD molecule is covered by *FUSE* (see Sembach (1999) for a complete list). H₂ column densities are significantly low in the LMC and contamination due to molecular hydrogen lines is non-significant for O VI measurements in the LMC. Absorption due to HD is about 4 orders weaker compared to H₂ transitions. Therefore, we neglect any contribution from HD molecule to the column densities of O VI in the LMC.

2.2 Measurement of O VI column densities

The measurement of equivalent widths and column densities of O VI absorption for all the lines of sight were done following Savage & Sembach (1991); Sembach & Savage (1992) and Howk et al. (2002a). This apparent optical depth technique (Savage & Sembach 1991) is now commonly used in the analysis of interstellar absorption lines and is applicable to cases with non-saturated absorption profiles. Briefly the technique uses an apparent optical depth in terms of velocity, i.e., an instrumentally blurred version of the true optical depth, given as

$$\tau_a(v) = \ln[I_o(v)/I_{obs}(v)], \quad (1)$$

where I_o is the estimated continuum intensity and I_{obs} is the intensity of the absorption line as a function of velocity. If the resolution of the instrument is very high compared to the FWHM of the absorption line, the apparent optical depth is a very good representation of the true optical depth. The apparent column density ($N_a(v)$ [atoms cm⁻² (km s⁻¹)⁻¹]) is calculated by the following relation

$$N_a(v) = \frac{m_e c \tau_a(v)}{\pi e^2 f \lambda} = 3.768 \times 10^{14} \frac{\tau_a(v)}{f \lambda}, \quad (2)$$

where λ is the wavelength (in Å) and f is the oscillator strength of the atomic species (for O VI, f value of 0.1325 has been adopted from Yan et al. (1998)). Similar to Howk et al. (2002a), we find that the 1032 Å O VI profile is broad and is fully resolved by *FUSE*. However, the weaker absorption of the O VI doublet at 1037.6 Å is found to be inseparable from the CII* and H₂ absorption.

The details of the apparent optical depth measurements are listed in Table 2. The overlap of the O VI absorption of the MW and the LMC does not allow a precise measurement of column densities for the LMC. For the

lines of sight (Sk-65D21, Sk-67D69, Sk-67D105, HV2543, Sk-66D100, HV5936, Sk-67D211, Sk-69D220, Sk-66D172, Sk-68D137, D301-1005, and D301-NW8) where the LMC O VI is distinct from the MW O VI, the limits of velocities over which integration was performed were easy to obtain. Taking cue from these lines of sight, we estimate the lower velocity limit for the lines of sight where the LMC O VI was not separated from the MW O VI. The errors in the equivalent widths and column densities are 1σ uncertainties derived using the uncertainty in the *FUSE* data and the fitting procedures. The principal contributor to these errors is the ambiguity in the continuum fitting of several of the spectra.

3 DISTRIBUTION AND PROPERTIES OF O VI IN THE LMC

3.1 Abundance and linewidth of O VI

The LMC spectra were selected based on the quality of the spectra around O VI spectral feature. The survey presented here has more-or-less complete coverage of the well known regions of the LMC such as 30 Doradus, N11, LMC 4, etc., and thus, is very useful in studying the variation of O VI at small scales as well. We find a significant amount of variation in the O VI column densities in a single region and in different regions of the LMC.

Our data cover a wide range of targets; O type stars, B type stars, Wolf-Rayet objects, supernova remnants, etc. The complete list of the background targets is provided in Table 1. These observations give fine details of the small scale structure of O VI column density in the LMC probing to a scale of ~ 10 pc in some regions. We find the O VI absorption in the LMC to be very patchy as is true for the MW. The O VI column density varies from the lowest value of 5.28×10^{13} atoms cm⁻² near a HII region (DEM 7) to the highest value of 3.74×10^{14} atoms cm⁻² just north of the LMC bar. Howk et al. (2002a) report the distribution of O VI in the LMC to be patchy as well with the log N(O VI) value in the LMC varying from 13.9 to 14.6 atoms cm⁻² and a mean of 14.37 atoms cm⁻². Their data did not provide any small scale variation in the column density of O VI with the smallest scale probed is about 450–500 pc.

Given the coverage of our data, we have studied the variation in O VI absorption in different regions of the LMC. We find that the 30 Doradus and SN 1987 A regions dominate in terms of the abundance of O VI. The mean and median values of log N(O VI) for targets in and around 30 Doradus and SNR 1987A are 14.30 and 14.27 atoms cm⁻² respectively. 30 Doradus is the largest HII region of LMC with a dense concentration of early type massive stars and has thus, attracted extensive research in different wavelength bands (Walborn et al. 1992; Parker 1993; Malumuth & Heap 1994; Walborn & Blades 1997; Townsley et al. 2006; Indebetouw et al. 2009). We discuss in detail about the O VI distribution and its properties in 30 Doradus region in section 5.

N11 region, which is associated with several OB associations and has a superbubble at its center, shows a high value of O VI column density. The mean of log N(O VI) in the N11 region is 14.21 atoms cm⁻².

Another interesting region is the LMC 4 Supergiant

shell that includes the Shapley Constellation III, which is one of the largest region associated with star formation (Dopita et al. 1985; Dolphin & Hunter 1998). The log $N(\text{O VI})$ value in LMC 4 supershell varies from a minimum of 13.86 atoms cm^{-2} to a maximum of 14.45 atoms cm^{-2} with a mean value of 14.20 atoms cm^{-2} and a median value of 14.25 atoms cm^{-2} . Other regions of the LMC also show patchiness in the O VI distribution. Statistically, the mean of the O VI column density in the LMC is 1.88×10^{14} atoms cm^{-2} which is lower than 2.34×10^{14} atoms cm^{-2} given by Howk et al. (2002) for 12 lines of sight. The difference is most likely due to the wide coverage of background targets in our data. The median value of the O VI column density is 1.66×10^{14} atoms cm^{-2} which also is less than the value reported by Howk et al. (2002a). Overall we find that there is an ubiquitous presence of O VI throughout the LMC.

The kinematics of O VI in the LMC is difficult to study because of the ambiguity in separating the LMC O VI absorption from the MW absorption. For some of the *FUSE* targets, i.e., for Sk-65D21, Sk-67D69, Sk-67D105, HV2543, Sk-66D100, HV5936, Sk-67D211, Sk-69D220, Sk-66D172, Sk-68D137, D301-1005, and D301-NW8, O VI absorption at LMC velocities are distinct from the MW (Fig. 3). Linewidth for the LMC O VI profiles are obtained with relatively less error for these lines of sight. The LMC O VI absorption profiles have all been fitted with a single Gaussian. The corresponding FWHM for these lines of sight are 55, 85, 78, 90, 90, 113, 100, 85, 105, 94, 107, and 91 km s^{-1} respectively. The temperature range estimated from these widths is $T \sim 1 \times 10^6 - 5 \times 10^6$ K. O VI abundance is maximum at a temperature of 3×10^5 K, thus, higher FWHM of these profiles is probably due to other broadening mechanisms such as more than one velocity component and/or collision and turbulence. This also represents the kinematic flow structure of O VI in the LMC.

The linewidth for the MW O VI profiles are narrower than the LMC profiles (Savage et al. 2003; Oegerle et al. 2005; Savage & Lehner 2006). For the Galactic halo, Savage et al. (2003) report a range for σ (linewidth) from 16 to 65 km s^{-1} (corresponding FWHM range is 38–153 km s^{-1}). Oegerle et al. (2005), for the local ISM, report average σ to be 16 km s^{-1} (FWHM = 38 km s^{-1}) while Savage & Lehner (2006) report σ values ranging from 15 km s^{-1} to 36 km s^{-1} (FWHM ranging from 35 km s^{-1} to 85 km s^{-1}). The linewidth of the SMC O VI absorption profile are comparable to that of the LMC. The FWHM range for the SMC O VI absorption is from 82 to 115 km s^{-1} with a mean of 94 km s^{-1} (Hoopes et al. 2002). We obtained a mean FWHM value of 91 km s^{-1} for the LMC selected lines of sight. Howk et al. (2002a) have compared O VI absorption profiles of the LMC with Fe II absorption and find that the Fe II profiles are much narrower suggesting that the thermal broadening effect for O VI absorption is much more significant.

3.2 Comparison with the MW and the SMC

The MW and the SMC offer a different ISM environment compared to the LMC especially due to the difference in the metallicity. The absorption profiles of the MW O VI are different from the LMC O VI and sometimes these profiles are

difficult to separate in an unambiguous manner, thus, a comparison of the kinematics is not possible. Howk et al. (2002a) have compared the O VI absorption with Fe II absorption at 1125.45 Å (fig. 9 in Howk et al. (2002a)). While, the Fe II profiles for the MW and the LMC are clearly separated from each other, the O VI absorption suffers an overlap. This is due to the difference in width of the two absorption. The overlap of the MW O VI absorption profile with the LMC O VI absorption constrained Howk et al. (2002a) to arrive at a definite conclusion about the existence of outflows from the LMC. Following the discussion about the distribution of O VI in the LMC in the previous section, we now present an overview of O VI in the MW and the SMC.

O VI in the MW has been extensively studied since the launch of *FUSE* (Savage et al. 2000; Howk et al. 2002b; Wakker et al. 2003; Savage et al. 2003; Oegerle et al. 2005; Savage & Lehner 2006; Bowen et al. 2008). Savage et al. (2000) were the first to study the O VI absorption in the disk and halo of the MW as seen towards 11 extragalactic objects (active galactic nuclei) using *FUSE*, confirming the large scale presence of hot gas in the halo (Spitzer 1956). The authors find that $\log N_{\perp}(\text{O VI})$ varies from 13.80 to 14.64 atoms cm^{-2} and the distribution of O VI is quite patchy. To compare with the projected O VI column density on the plane of the MW, we calculated the projection of O VI column on to the plane of the LMC. Taking the inclination angle of the LMC to be 33° , we find the mean value of $\log N_{\perp}(\text{O VI}) \equiv \log N(\text{O VI}) \cos \theta = 14.16$ atoms cm^{-2} . Savage et al. (2000) quote a mean value of 14.29 atoms cm^{-2} for their sample. The median value of our sample is 14.14 atoms cm^{-2} , while for the Savage et al. (2000) sample, it is 14.21 atoms cm^{-2} .

Savage et al. (2003) report *FUSE* observations of O VI absorption towards 100 extragalactic lines of sight to study the properties and distribution of O VI in the galactic halo. The average $\log N(\text{O VI})$ for the complete sample is 14.36 atoms cm^{-2} while $\log N(\text{O VI}) \sin |b|$ value for the complete sample is 14.21 atoms cm^{-2} . The results reveal that there are substantial differences in the values of $\log N(\text{O VI})$ and $\log N(\text{O VI}) \sin |b|$ in the northern Galactic hemisphere compared to the southern Galactic hemisphere. The patchiness in the distribution of O VI absorption is found to be similar over angular scales extending from $\leq 1^{\circ}$ to 180° . An extensive survey of O VI in the MW disk has been reported by Bowen et al. (2008) in which the authors have studied O VI column density towards 148 early type stars. The correlation between O VI column density and effective distance to a star establishes the fact that the O VI is interstellar in nature and points to the universal presence of the interstellar phenomena that gives rise to O VI throughout the Galaxy.

Hoopes et al. (2002) have surveyed O VI absorption towards 18 early type stars in the SMC and report a widespread presence of O VI. The mean value of $\log N(\text{O VI})$ in the SMC is 14.53, which is higher than the LMC and the MW values. The O VI column density in the SMC correlates with the distance from NGC 346, a star forming region that shows the highest abundance of O VI in the SMC.

3.3 Comparison with X-ray and $\text{H}\alpha$

The LMC has been the focus of $\text{H}\alpha$ and X-ray surveys to search for ionized structures in the ISM. $\text{H}\alpha$ surveys have

revealed the presence of HII regions, supernova remnants, and large scale structures including superbubbles and super-shells (Davies et al. 1976), whereas, X-ray observations have been done to study bright X-ray sources (Trumper et al. 1991), the hot gas in the ISM (Wang et al. 1989, 1991) and diffuse X-ray emission (Bomans et al. 1994). Since O VI traces the ISM gas with temperatures $\sim 10^5$ K, which is at the interface between hot gas (temperature $\geq 10^6$ K) traced by X-rays and warm gas (temperature $\sim 10^4$ K) traced by H_α , correlation between O VI abundance and X-ray and H_α emissions is expected.

The O VI observations cover specific regions of the LMC with varying environmental conditions. To get an idea about the variation of O VI column densities with different environments in the LMC, we have overlaid O VI column densities as circles on H_α image (Gaustad et al. (2001); Fig. 5). The diameter of the circle is linearly proportional to $\log N(\text{O VI})$. Interestingly, it is noted that O VI abundance is high in regions with low H_α and X-ray emissions, i.e., regions that are relatively inactive. However, regions like superbubbles are O VI rich, for e.g., 30 Doradus C and N11. The gross picture suggests that O VI does not correlate with either H_α or X-ray emissions. We have plotted $\log N(\text{O VI})$ against \log relative H_α and X-ray surface brightnesses to have a better insight. The X-ray surface brightness is obtained from *ROSAT* PSPC mosaic image of the LMC covering the energy range 0.5–2.0 keV (Snowden & Petre 1994). Figures 6 and 7 show the correlation of $\log N(\text{O VI})$ with H_α and X-ray surface brightnesses for the LMC barring five lines of sight in the X-ray correlation plot. Four of the excluded lines of sight (Sk-67D250, D301-1005, D301-NW8 and Sk-65D63) are not covered by the X-ray observations and one (Sk-69D257) has extremely high X-ray emission (about 2 orders of magnitude higher than other lines of sight). The H_α and X-ray surface brightness are measured by re-binning the corresponding images to increase the signal to noise. The lack of correlation is evident in both plots, as also found by Howk et al. (2002a). Since, H_α traces warm ISM and star formation, there seems to be no direct relation between O VI formation and these processes. A better correlation with X-ray is expected as the hot gas traced by X-ray is presumed to cool through temperatures where O VI formation takes place. There is a high abundance of O VI in supernova remnants and superbubbles of the LMC, whereas, bright X-ray emission is observed mostly from the supernova remnants of the LMC. X-ray emission associated with supernova remnants in the LMC is a factor of 2 to 3 times greater than the X-ray emission associated with supergiant shells and the Bar in the LMC (Points et al. 2001).

4 O VI IN SUPERBUBBLES OF THE LMC

Superbubbles may be formed due to the strong stellar wind from young stars and/or supernova explosions forming a local cavity in the surrounding ISM. These are excellent examples of the interaction of young hot stars and the ISM. Superbubbles contain hot gas ($\sim 10^6$ K) that is heated by shocks created by stellar winds (Castor et al. 1975; Weaver et al. 1977; Chu & Mac Low 1990), which is an ideal condition for the formation of O VI. The LMC hosts more than 20 superbubbles and recently O VI has been detected in a su-

perbubble N70 (Danforth & Blair 2006), where they have reported around 60% excess in abundance of O VI in comparison to non-superbubble lines of sight in the proximity of N70. The authors conclude that superbubbles act as local O VI reservoirs and have a different absorption profile compared to the non-superbubble O VI absorption profiles. They find that the O VI is formed by the thermal conduction between the interior hot X-ray producing gas and the cool photo-ionized shell of N70. Sankrit & Dixon (2007) have detected O VI in emission in several superbubbles in the LMC further emphasizing that superbubbles are important contributors to the overall O VI budget.

We have 22 O VI observations covering 10 superbubbles. Of the 22 observations, 3 are in N70 (Sk-67D250, D301-1005 and D301-NW8) which have already been reported by Danforth & Blair (2006) and 4 are in N144, N204, N206 and N154 respectively which have been discussed by Howk et al. (2002a). We report 15 new observations of O VI absorption in the superbubbles 30 Doradus C, N158, N11, N51, and N57. Significant variation in O VI abundance exists towards these lines of sight. The minimum value of $\log N(\text{O VI})$ is 14.04 atoms cm^{-2} in superbubble N206 and the maximum value of $\log N(\text{O VI})$ is 14.57 atoms cm^{-2} in superbubble N70. The properties of O VI in superbubbles reported here are tabulated in Table 3. Comparing the abundance of O VI for the superbubble and non-superbubble lines of sight, we find that the mean $\log N(\text{O VI})$ for superbubble lines of sight is $\langle N_{SB} \rangle = 14.35$ atoms cm^{-2} while for the non-superbubble lines of sight this is $\langle N_{non-SB} \rangle = 14.19$ atoms cm^{-2} . Thus, an excess O VI abundance of about 40% in superbubbles of the LMC is found in comparison to non-superbubble regions. Combining the Danforth & Blair (2006) and Howk et al. (2002a) data for superbubble and non-superbubble lines of sight (excluding Sk-67D05 sightline; see Howk et al. (2002a) for details), the O VI excess in superbubbles is about 46%, which is comparable to our results. Thus, results reported here support and confirm that superbubbles do show higher O VI abundance in comparison to the general halo absorption seen in other LMC lines of sight. Some of the non-superbubble lines of sight show an enhanced O VI column density owing to local effects. Lehner & Howk (2007) compared superbubble and non-superbubble lines of sight for the LMC and found that some quiescent environments showed an enhanced O VI abundance, sometimes even larger than that of superbubbles.

Even in a single superbubble, there are significant variations in the O VI column densities. We have four observations each for the superbubbles 30 Doradus C and N11. In the case of 30 Doradus C, we find that the variation in $N(\text{O VI})$ is more than a factor of 2 (from the minimum value of $N(\text{O VI})$ to the maximum value). For N11, this variation is about a factor of 2.5. The variation in $N(\text{O VI})$ for N70 is not much (for the three lines of sight included here) and this corroborates with the Danforth & Blair (2006) data.

5 PROPERTIES OF O VI IN 30 DORADUS

The 30 Doradus region of the LMC is ideally suited to study the interaction between a high rate of star formation and the surrounding ISM. This region is dominated by the star forming cluster NGC 2070 that contains the very interesting

star cluster R136 at the center. The proximity to 30 Doradus has allowed extensive research on the stellar content (Parker 1992; Parker & Garmany 1993; Walborn & Blades 1997) and initial mass function (Andersen et al. (2009) and references therein). 30 Doradus has also been investigated in detail in the infrared bands to study the dust properties (Sturm et al. 2000; Vermeij et al. 2002; Meixner et al. 2006). Indebetouw et al. (2009) studied the 30 Doradus in the mid-infrared wavelength band to determine the physical conditions of the ionized gas and found that the local effects of hot stars in 30 Doradus appear to dominate over any large-scale trend with distance from the central cluster R136.

The O VI abundance in 30 Doradus is higher than in other regions of the LMC with the highest value of $\log N(\text{O VI})$ being 14.56 atoms cm^{-2} near the center of the cluster R136. Fig. 8 shows the change in the $\log N(\text{O VI})$ values from the center of R136 up to an angular distance of 1 degree. We find an overall decrease in the O VI abundance away from the center of R136. An interpretation of this plot could be that the processes involved in the formation of O VI are likely to be associated with stellar radiation field but local effects cannot be neglected on a large angular scale. It should be noted that we do not find any correlation between O VI absorption and $\text{H}\alpha$ emission for LMC and thus, no relation between star formation is established on a larger scale.

As noticed earlier, $\log N(\text{O VI})$ does not correlate with X-ray emission for the LMC as a whole but surprisingly there is a good correlation for the 30 Doradus lines of sight (Fig. 9). The correlation is between $\log N(\text{O VI})$ and X-ray emission from 30 Doradus considering all the lines of sight within 1 degree around R136 except for one sightline (SK-69D257) that has exceptionally high value of X-ray surface brightness. One of the reasons for such high X-ray emission from SK-69D257 is its proximity to a high mass X-ray binary LMC X-1 (Points et al. 2001). The correlation in 30 Doradus suggests that O VI observed in this region is present in the ISM gas surrounding the X-ray emitting plasma, which may be due to the compactness, high density and non-uniform structure of 30 Doradus. The correlation confirms that the X-ray emitting gas cools through temperatures where O VI is being formed and supports the general consensus about the formation of O VI by collisional ionization in the interface regions between cooler photo-ionized ISM gas and hot exterior ISM gas (Slavin & Frisch 2002; Indebetouw & Shull 2004).

6 SUMMARY & CONCLUSIONS

We have presented O VI column density measurements for the LMC using *FUSE* data for 70 lines of sight. This is the widest coverage of the LMC to date. The results reported here reveal significant variation in O VI column densities over a very small angular scale thus confirming the patchiness of O VI distribution in the LMC. The most important inferences drawn from this work are following:

(i) This survey probes 70 lines of sight with varying environmental conditions. We find strong O VI absorption in the LMC that is not restricted to active regions. High O VI

abundance is present even in relatively inactive regions of the LMC.

(ii) There are significant variations in the velocity profiles of O VI absorption. The O VI absorption profile is broader than the MW absorption for many lines of sight but it should be noted that unambiguous separation of the MW and the LMC components is not possible for most of the lines of sight. This proves to be a significant hurdle in interpreting exact kinematics for O VI in the LMC (for e.g. outflows from the LMC, etc.).

(iii) The maximum column density measured for the LMC is $\log N(\text{O VI}) = 14.57$ atoms cm^{-2} and minimum value is $\log N(\text{O VI}) = 13.72$ atoms cm^{-2} . The mean value of O VI column density is $\langle \log N(\text{O VI}) \rangle = 14.23$ atoms cm^{-2} , which is slightly lower than the earlier reported value. The median value of O VI column density in the LMC comes to be 14.22 atoms cm^{-2} . The results corroborates with the previous finding that the distribution of O VI in the LMC is patchy.

(iv) Despite the fact that the LMC has lower metallicity than the MW, the abundance of O VI and properties of O VI absorption are similar in both the galaxies. The mean of $\log N_{\perp}(\text{O VI})$ value for the MW is 14.29 atoms cm^{-2} while the projected column density for the LMC, i.e., $\log N_{\perp}(\text{O VI})$ is 14.15 atoms cm^{-2} . A more extensive study for the MW suggests this value to be 14.21 atoms cm^{-2} . The SMC with even lower metallicity has higher O VI abundance with mean $\log N(\text{O VI}) = 14.53$ atoms cm^{-2} .

(v) O VI absorption in the LMC does not correlate with $\text{H}\alpha$ (warm gas) or X-ray (hot gas) emission but we find a good correlation between O VI absorption and X-ray emission in the 30 Doradus region. It is also seen that the O VI absorption is decreasing with increasing angular distance from the star cluster R136 suggesting some correlation with stellar radiation field.

(vi) The observations reported cover 10 superbubbles of the LMC and for 5 superbubbles (30 Doradus C, N158, N51, N11 and N57) O VI absorption is reported for the first time. Superbubbles are O VI rich and have 40% excess compared to non-superbubble lines of sight.

ACKNOWLEDGMENTS

AP and NVS acknowledge fellowships from the Department of Science and Technology, New Delhi. This research has made use of *Far Ultraviolet Spectroscopic Explorer* data. *FUSE* was operated by Johns Hopkins University for NASA. We acknowledge the use of Multimission Archive at Space Telescope Science Institute (MAST) and NASA Astrophysics Data System (ADS).

REFERENCES

- Andersen M., Zinnecker H., Moneti A., McCaughrean M. J., Brandl B., Brandner W., Meylan G., Hunter D., 2009, *ApJ*, 707, 1347
 Bernard J. P. et al., 2008, *AJ*, 136, 919
 Blair W. P., Oliveira C., Lamassa S., Gutman S., Danforth C. W., Fullerton A. W., Sankrit R., Gruendl R., 2009, *PASP*, 121, 634

- Bomans D. J., Dennerl K., Kurster M., 1994, *A&A*, 283, L21
- Bothun G. D., Thompson I. B., 1988, *AJ*, 96, 877
- Bowen D.V. et al., 2008, *ApJS*, 176, 59
- Castor J., McCray R., Weaver R., 1975, *ApJ*, 200, L107
- Chu Y. -H., Mac Low M. -M., 1990, *ApJ*, 365, 510
- Conti P. S., Garmany C. D., Massey P., 1986, *AJ*, 92, 48
- Cole A. A., Nordsieck K. H., Gibson S. J., Harris W. M. 1999a, *AJ*, 118, 2280
- Cole A. A., Wood K., Nordsieck K. H. 1999b, *AJ*, 118, 2292
- Cox, D. P., 2005, *ARA&A*, 43, 337
- Danforth C. W., Howk J. C., Fullerton A. W., Blair W. P., Sembach K. R., 2002, *ApJS*, 139, 81
- Danforth C. W., Shull J. M., 2005, *ApJ*, 624, 555
- Danforth C. W., Shull J. M., Rosenberg J. L., Stocke J. T., 2006, *ApJ*, 640, 716
- Danforth C. W., Blair W. P., 2006, *ApJ*, 646, 205
- Davies R. D., Elliott K. H., Meaburn J., 1976, *MNRAS*, 81, 89
- Dixon W. Van D., Hurwitz M, Ferguson H. C., 1996, *ApJ*, 469, L77
- Dixon W. V. D., Sankrit R., Otte B., 2006, *ApJ*, 647, 328
- Dixon W. V. D. et al., 2007, *PASP*, 119, 527
- Dixon W. V. D, Sankrit R., 2008, *ApJ*, 686, 1162
- Dolphin A. E., Hunter D. A., 1998, *AJ*, 116, 1275
- Dopita M. A., Mathewson D. S., Ford V. L., 1985, *ApJ*, 297, 599
- Edgar R. J., Chevalier R. A., 1986, *ApJ*, 310, L27
- Feast M., 1999, in Chu Y. -H., Suntzeff N., Hesser J., Bohlender D., eds, *New Views of the Magellanic Clouds*, IAU Symp., 190, 542
- Fitzpatrick E. L., 1988, *ApJ*, 335, 703
- Friedman S. D. et al., 2000, *ApJ*, 538, L39
- Garmany C. D., Walborn N. R., 1987, *PASP*, 99, 240
- Gaustad J. E., McCullough P. R., Rosing W., Van Buren D., 2001, *PASP*, 113, 1326
- Grimes J. P. et al., 2009, *ApJS*, 181, 272
- Heckman T. M., Norman C. A., Strickland D. K., Sembach K. R., 2002, *ApJ*, 577, 691
- Hoopes C. G., Sembach K. R., Howk J. C., Savage B. D., Fullerton A. W., 2002, *ApJ*, 569, 233
- Howk J. C., Sembach K. R., Savage B. D., Massa D., Friedman S. D., Fullerton A. W., 2002a, *ApJ*, 569, 214
- Howk J. C, Savage Blair D., Sembach K. R., Hoopes, C. G., 2002, *ApJ*, 572, 264
- Indebetouw R., Shull J. M., 2004, *ApJ*, 605, 205
- Indebetouw R. et al., 2009, *ApJ*, 694, 84
- Jenkins E. B., 1978a, *ApJ*, 219, 845
- Jenkins E. B., 1978b, *ApJ*, 220, 107
- Kim S., Staveley-Smith L., Dopita M. A., Sault R. J., Freeman K. C., Lee Y., Chu, Y. -H., 2003, *ApJS*, 148, 473
- Lehner N., Fullerton A. W., Sembach K. R., Massa D. L., Jenkins E. B., 2001, *ApJ*, 556, L103
- Lehner N., Fullerton A. W., Massa D., Sembach K. R., Zsargo, J., 2003, *ApJ*, 589, 526
- Lehner N., Howk J. C., 2007, *MNRAS*, 377, 687
- Malumuth E. M., Heap S. R., 1994, *AJ*, 107, 1054
- Massey P., Lang C. C., Degioia-Eastwood K., Garmany C. D., 1995, *ApJ*, 438, 188
- Massey P., Hunter D. A., 1998, *ApJ*, 493, 180
- Massey P., 2002, *ApJS*, 141, 81
- Meixner M. et al., 2006, *AJ*, 132, 2268
- Moffat A. F. J., Niemela V. S., Marraco H. G., 1990, *ApJ*, 348, 232
- Moos H. W. et al., 2000, *ApJ*, 538, L1
- Oegerle W. R., Jenkins E. B., Shelton R., Bowen D. V., Chayer P., 2005, *ApJ*, 622, 377
- Parker J. W., 1992, *PASP*, 104, 1107
- Parker J. W., 1993, *SSRv*, 66, 55
- Parker J. W., Garmany, C. D., 1993, *AJ*, 106, 1471
- Points S. D., Chu Y.-H., Snowden S. L., Smith R. C., 2001, *ApJS*, 136, 99
- Pradhan A. C., Pathak A., Murthy J., 2010, *ApJ*, 718, L141
- Rousseau J., Martin N., Prevot L., Rebeiro E., Robin A., Brunet J. P., 1978, *A&AS*, 31, 243
- Sahnow D. J. et al., 2000, *ApJ*, 538, L7
- Sankrit R., Dixon W. V. D., 2007, *PASP*, 119, 284
- Savage B. D., Sembach K. R., 1991, *ApJ*, 379, 245
- Savage B. D. et al., 2000, *ApJ*, 538, L27
- Savage B. D. et al., 2003, *ApJS*, 146, 125
- Savage B. D., Lehner N., 2006, *ApJS*, 162, 134
- Sembach K. R., Savage B. D., 1992, *ApJS*, 83, 147
- Sembach K.R., 1999, in Gibson, B. K., Putman, M. E. eds., *ASP Conf. Ser. 166, Stromlo Workshop on High Velocity Clouds (San Francisco:ASP)*, 243
- Shelton R., Cox D. P., 1994, *ApJ*, 434, 599
- Shelton R. L. et al., 2001, *ApJ*, 560, 730
- Shelton R. L., 2002, *ApJS*, 569, 758
- Slavin J. D., Frisch P. C., 2002, *ApJ*, 565, 364
- Smith L. F., Shara M. M., Moffat A. F. J., 1990, *ApJ*, 358, 229
- Smith L. F., Shara M. M., Moffat A. F. J., 1996, *MNRAS*, 281, 163
- Snowden S. L., Petre R., 1994, *ApJ*, 436, L123
- Spitzer L., 1956, *ApJ*, 124, 20
- Sturm E., Lutz D., Tran D., Feuchtgruber H., Genzel R., Kunze D., Moorwood A. F. M., Thornley M. D., 2000, *A&A*, 358, 481
- Torres-Dodgen A. V., Massey, P., 1988, *AJ*, 96, 1076
- Townsley L. K., Broos P. S., Feigelson E. D., Garmire G. P., Getman K. V., 2006, *AJ*, 131, 2164
- Trumper J. et al., 1991, *Nat*, 349, 579
- Tumlinson J. et al., 2002, *ApJ*, 566, 857
- van der Marel R. P., Cioni, M. -R. L., 2001, *AJ*, 122, 1807
- Vermeij R., Peeters E., Tielens A. G. G. M., van der Hulst J. M., 2002, *A&A*, 382, 1042
- Wakker B. P. et al., 2003, *ApJS*, 146, 1
- Walborn N. R., 1977, *ApJ*, 215, 53
- Walborn N. R., Ebbets D. C., Parker J. Wm., Nichols-Bohlin J., White R. L., 1992, *ApJ*, 393, L13
- Walborn N. R., Lennon D. J., Haser S. M., Kudritzki R. -P., Voels S. A., 1995, *PASP*, 107, 104
- Walborn N. R., Blades J. C., 1997, *ApJS*, 112, 457
- Walborn N. R. et al., 2002a, *AJ*, 123, 2754
- Walborn N. R. et al., 2002b, *ApJS*, 141, 443
- Wang Q., Hamilton T., Helfand D. J., 1989, *Nat*, 341, 309
- Wang Q., Hamilton T., Helfand D. J., Wu X., 1991, *ApJ*, 374, 475
- Weaver R., McCray R., Castor J., Shapiro P., Moore R., 1977, *ApJ*, 218, 377
- Welsh B. Y., Lallement R., 2008, *A&A*, 490, 707
- Yan Z. -C., Tambasco M., Drake G. W. F., 1998, *Phys. Rev. A*, 57, 1652

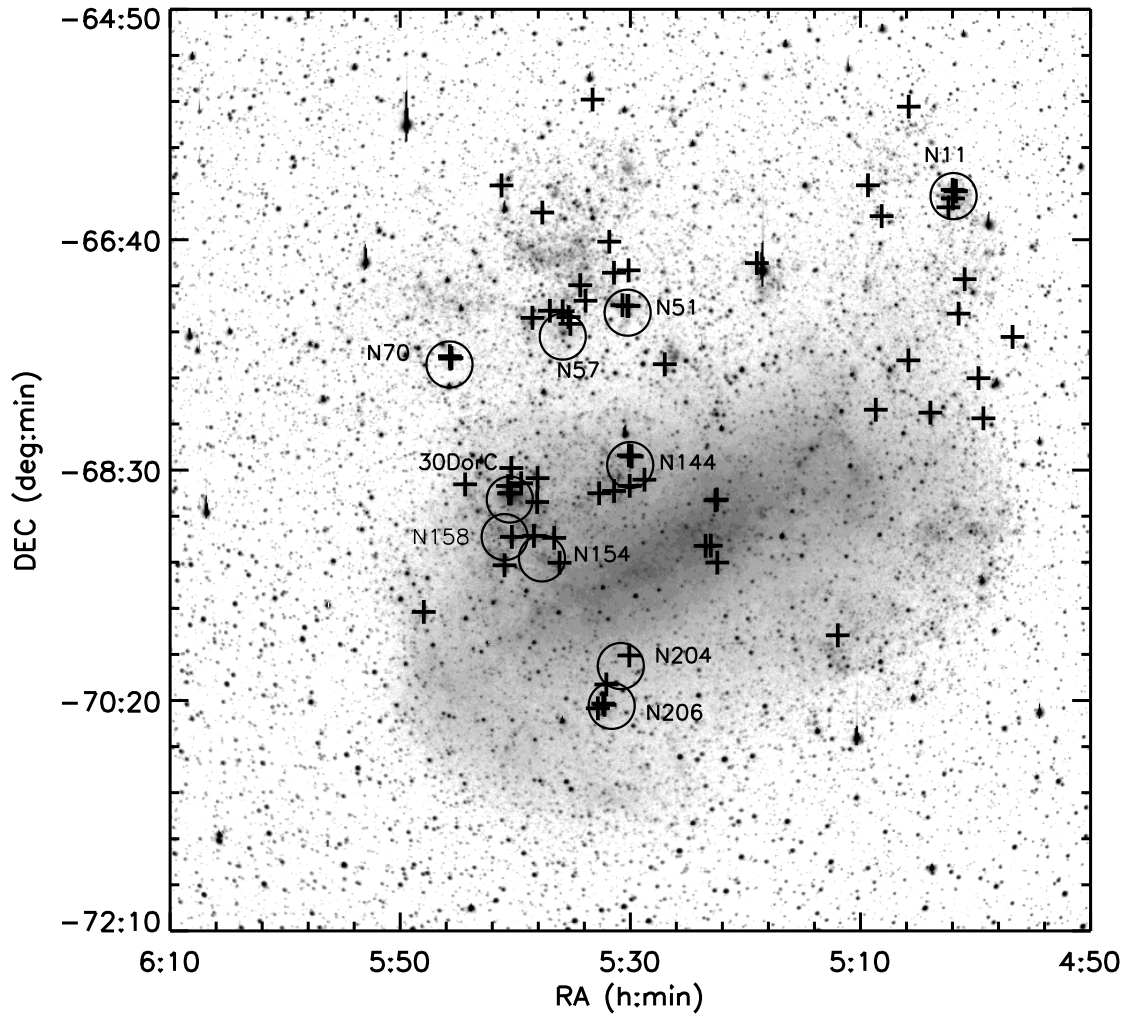


Figure 1. R-band image of the LMC (Bothun & Thompson 1988) showing the targets towards which O VI absorption have been studied. Superbubbles have been shown by circles.

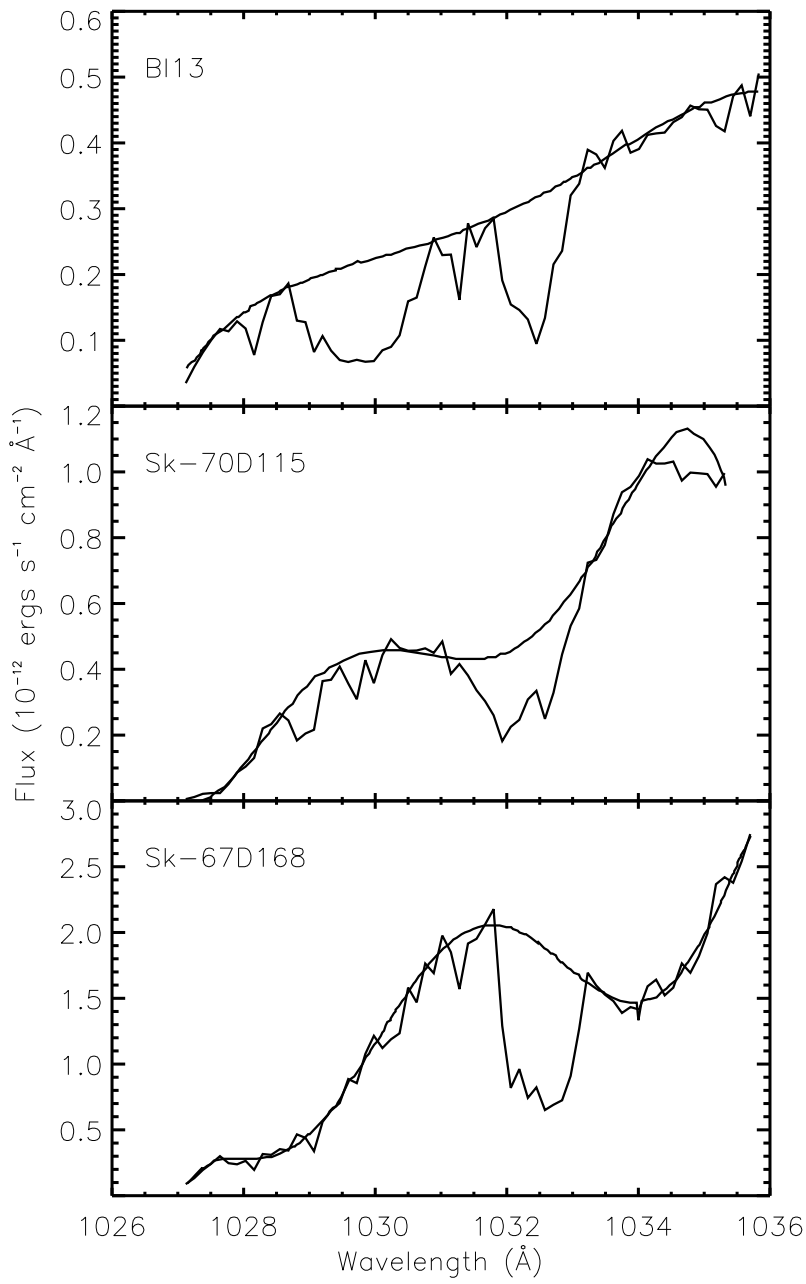
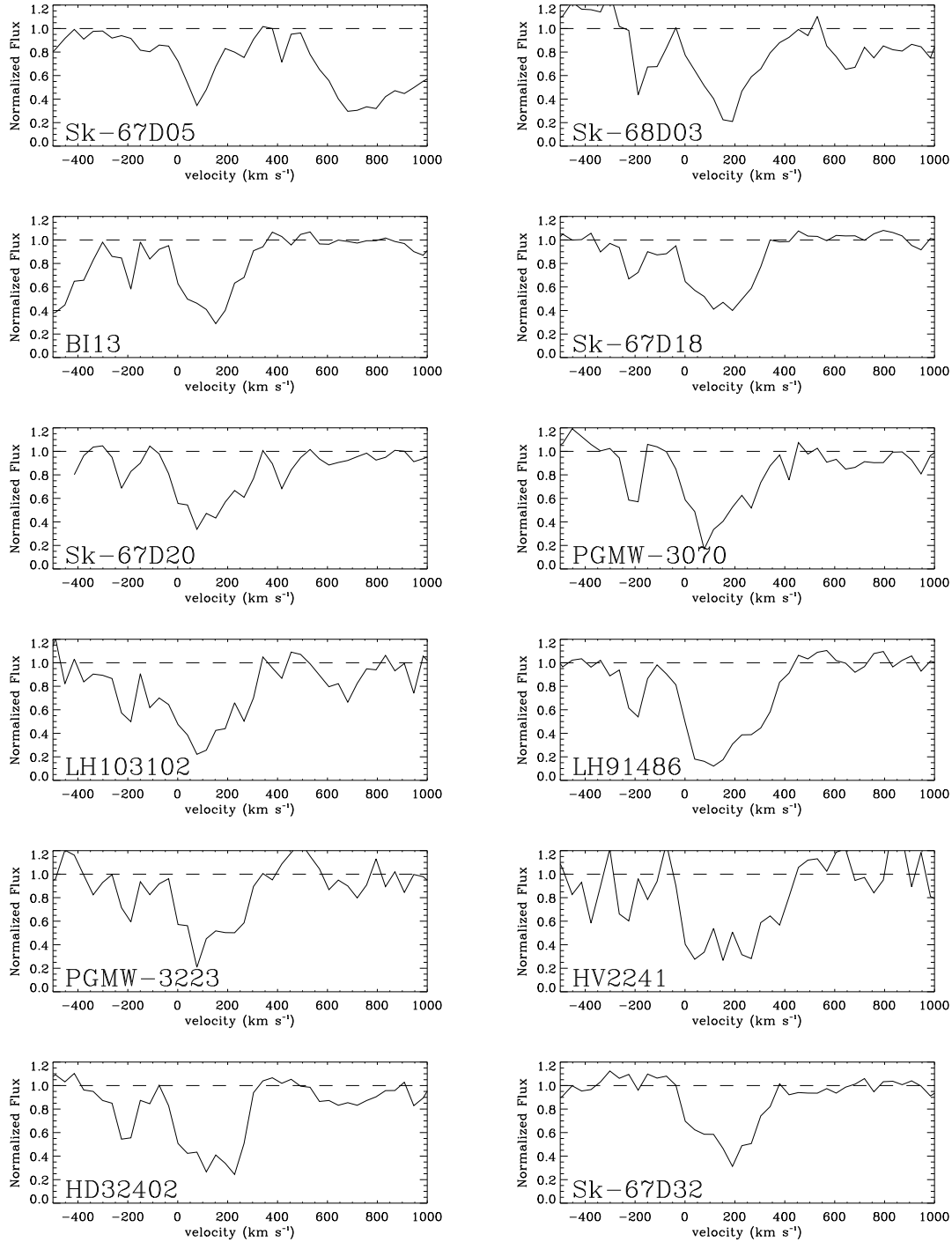
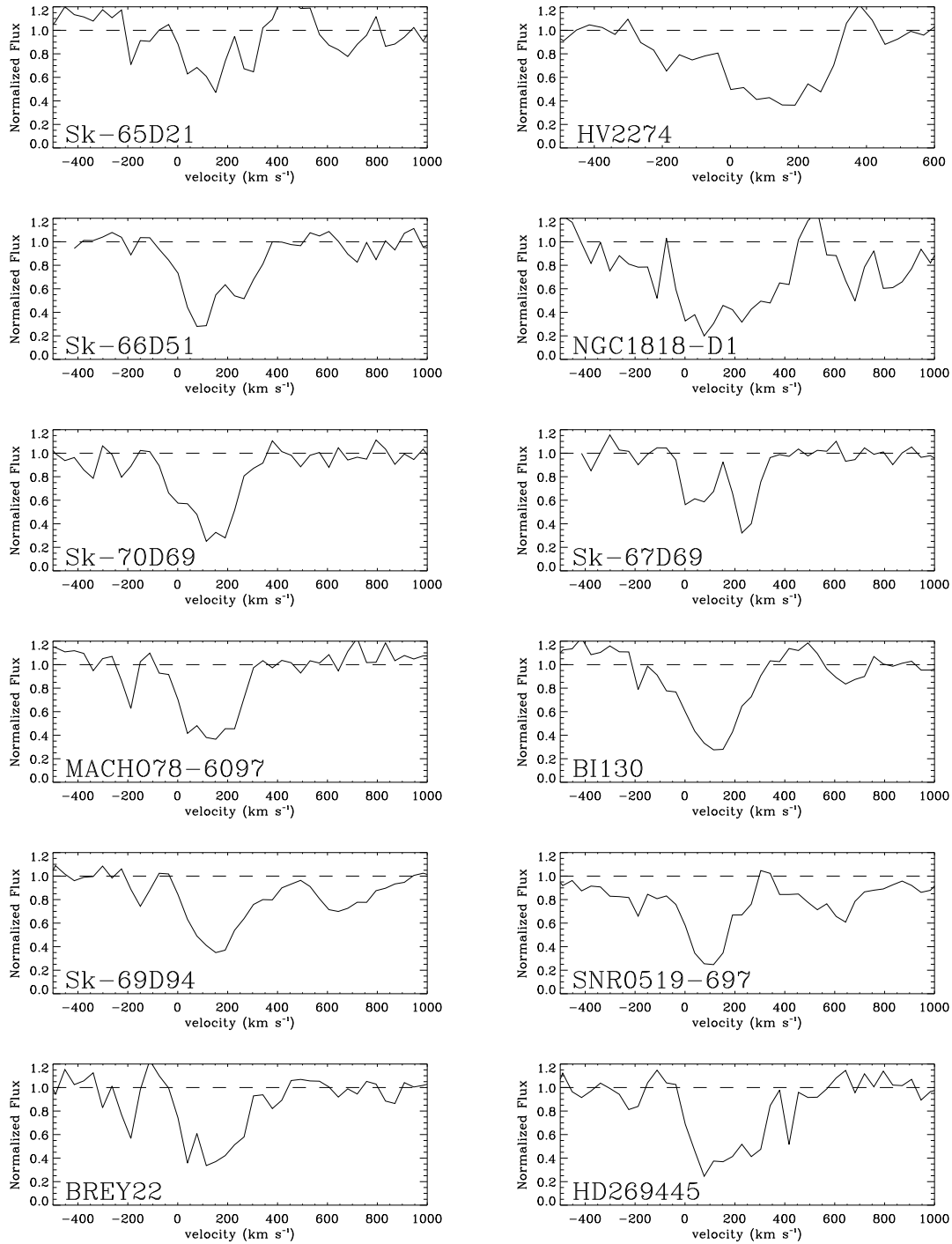


Figure 2. Examples for continuum fitting for three sightlines in the region near O VI absorption at 1031.92 Å. The top to bottom panels show the increasing complexity of fitting the stellar continuum.



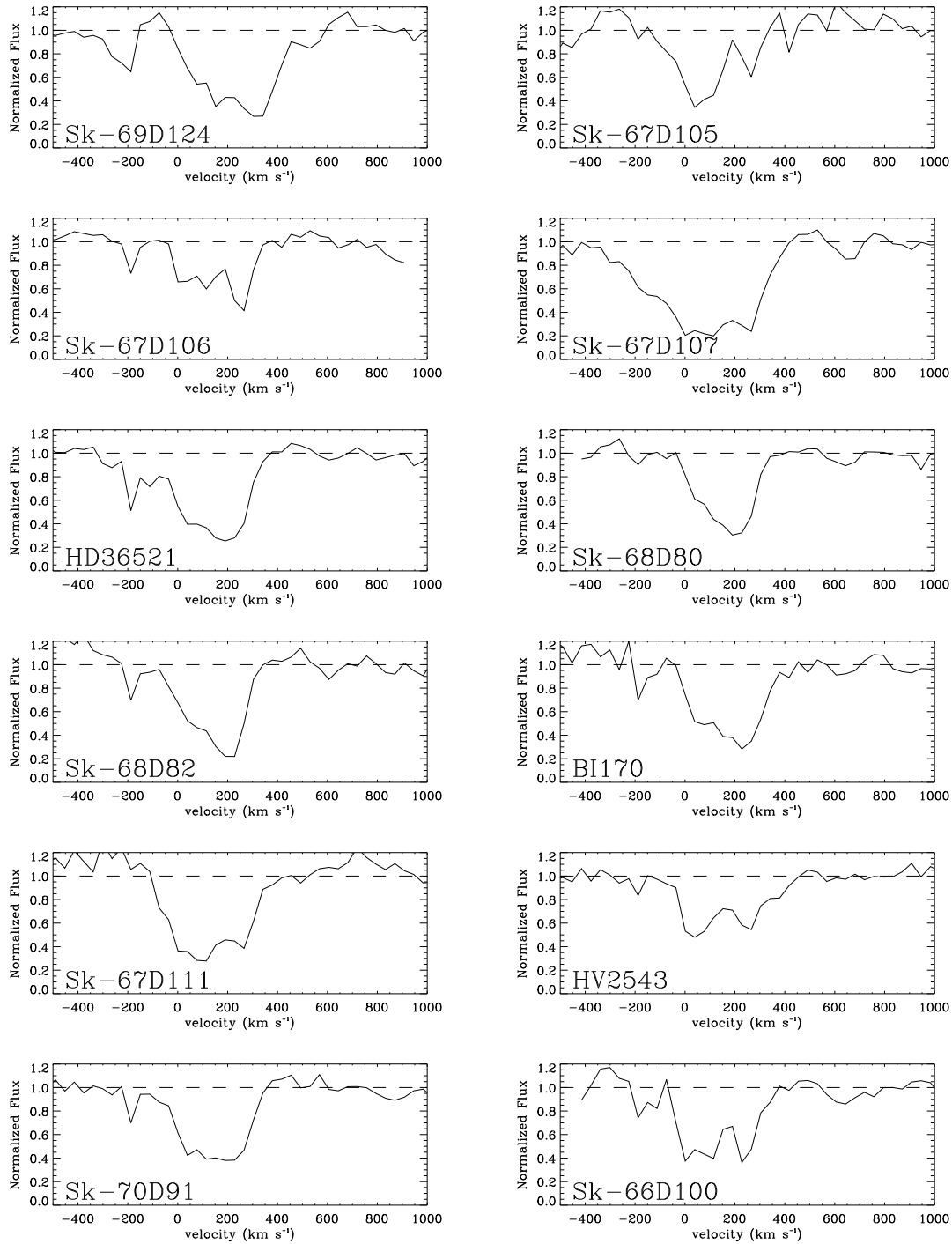
(a) Normalized O VI absorption profiles for the 70 lines of sight. Table 1 gives the details of each sightline.

Figure 3.



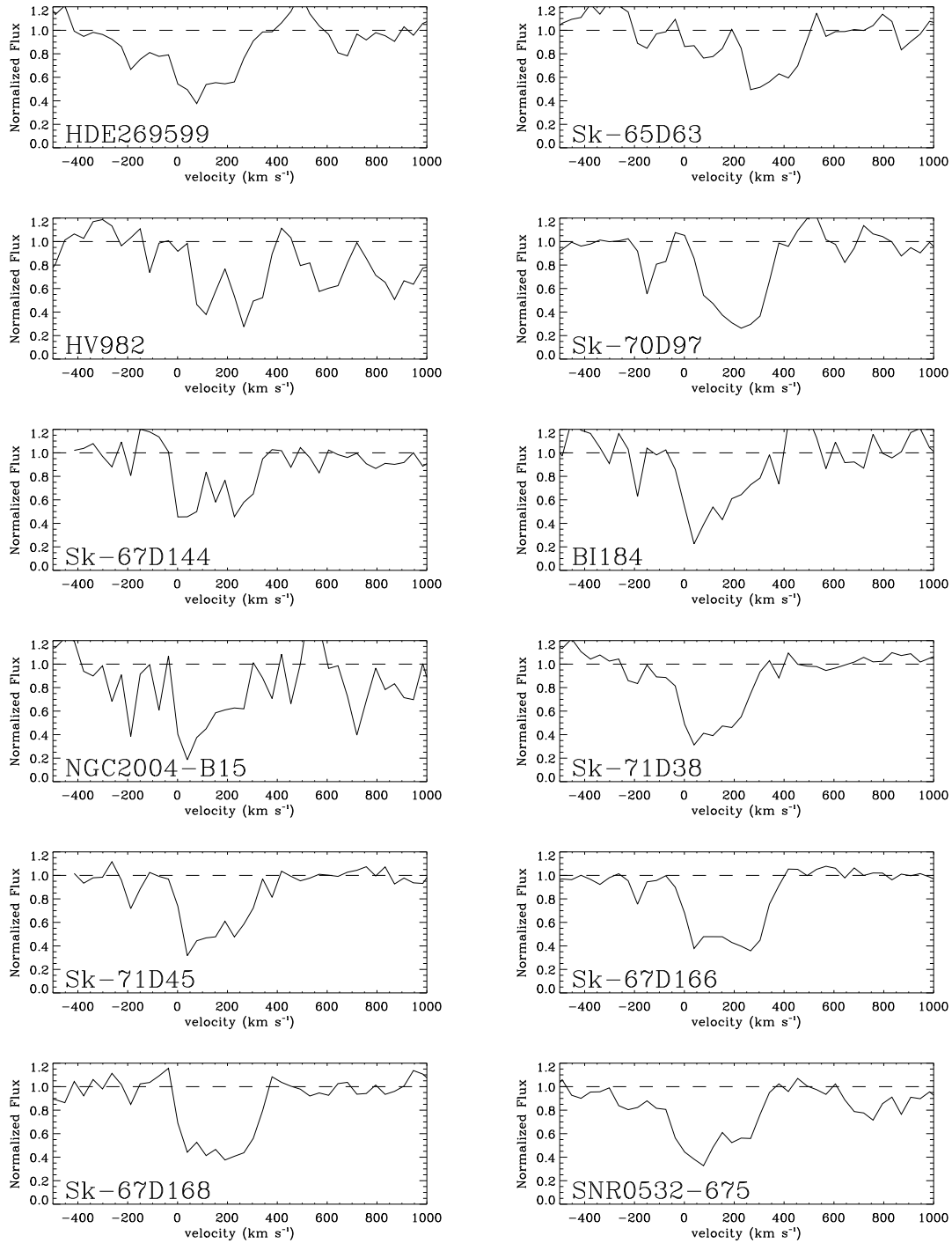
(b) Same as Fig. 3(a)

Figure 3.



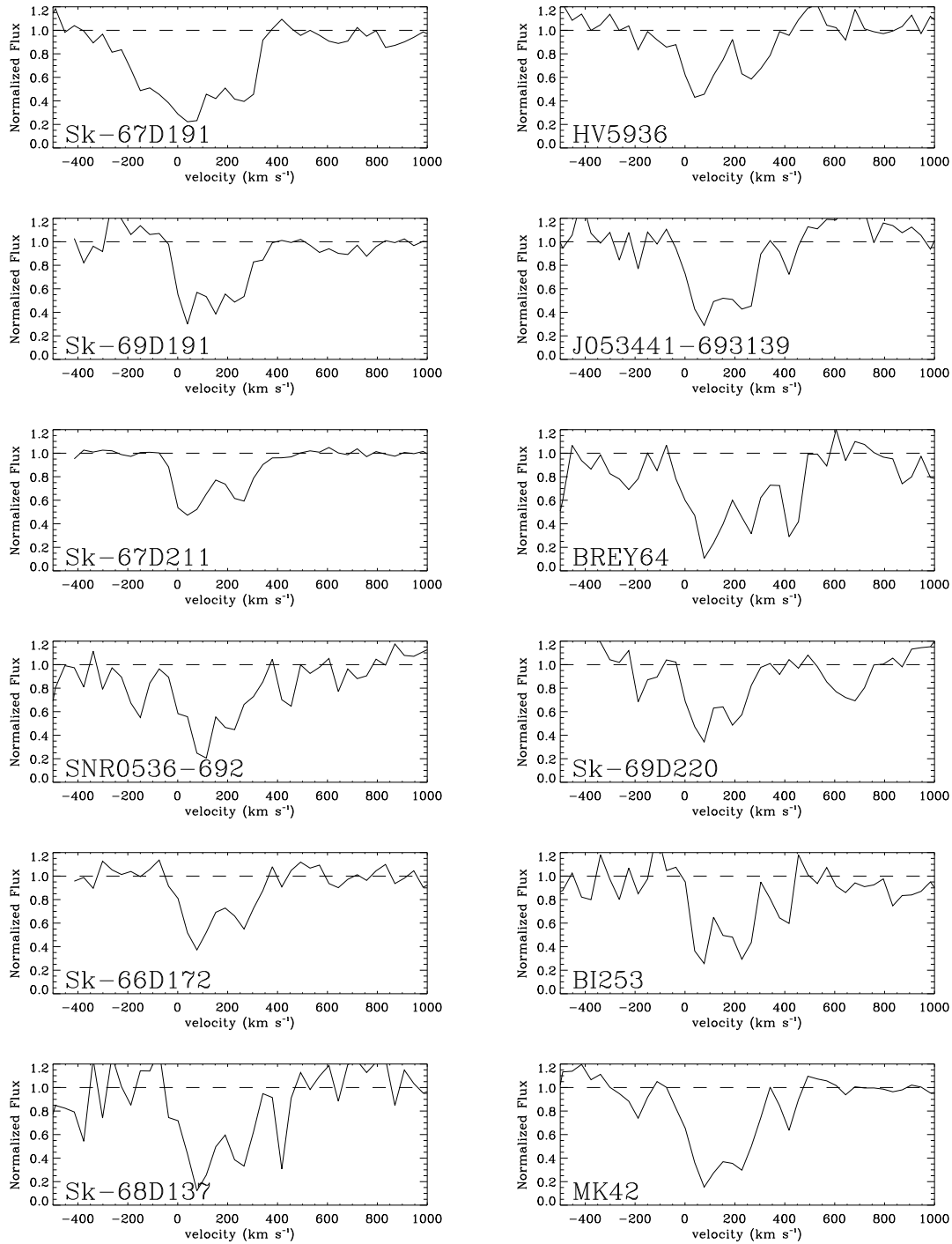
(c) Same as Fig. 3(a)

Figure 3.



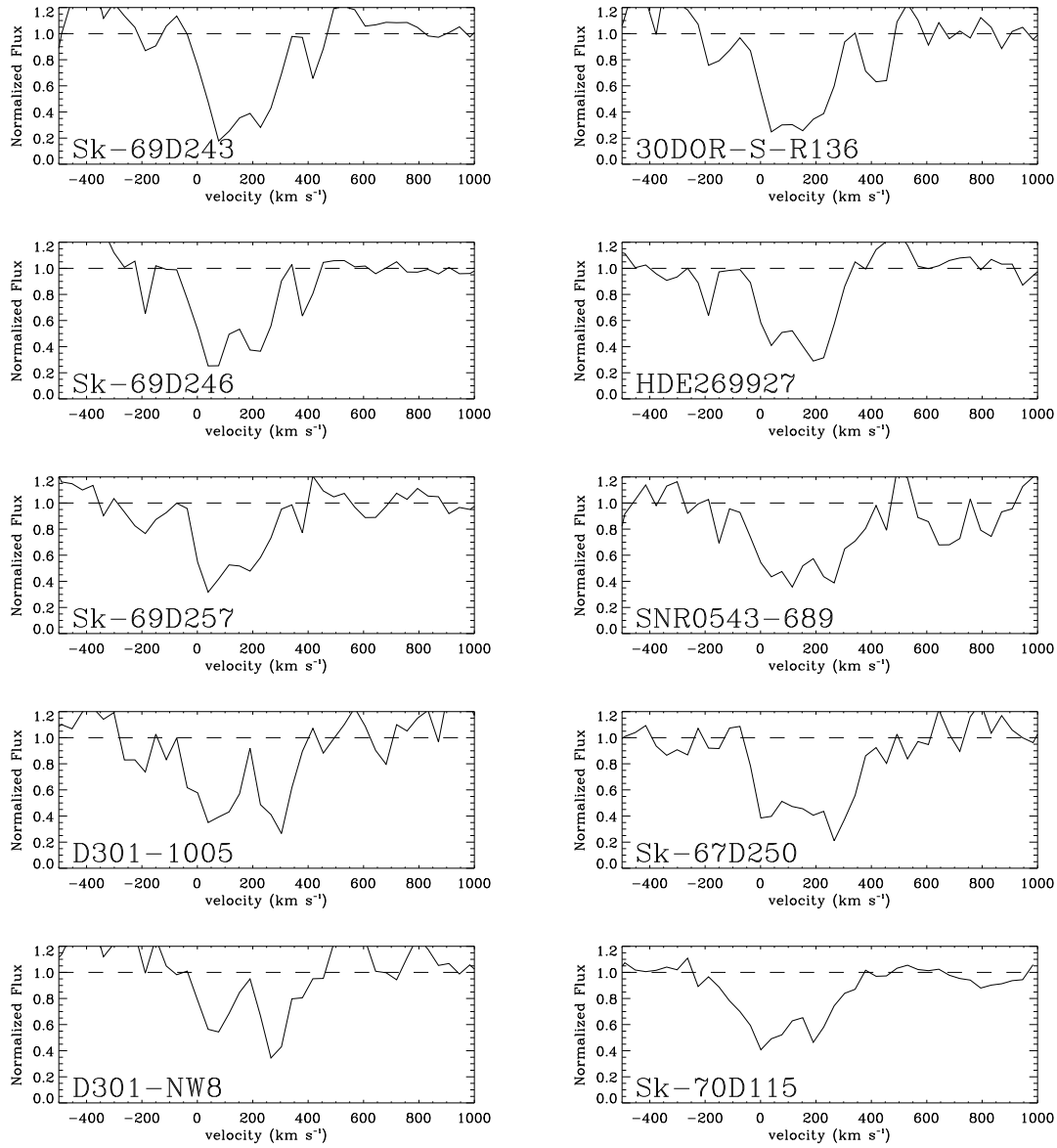
(d) Same as Fig. 3(a)

Figure 3.



(e) Same as Fig. 3(a)

Figure 3.



(f) Same as Fig. 3(a)

Figure 3. *

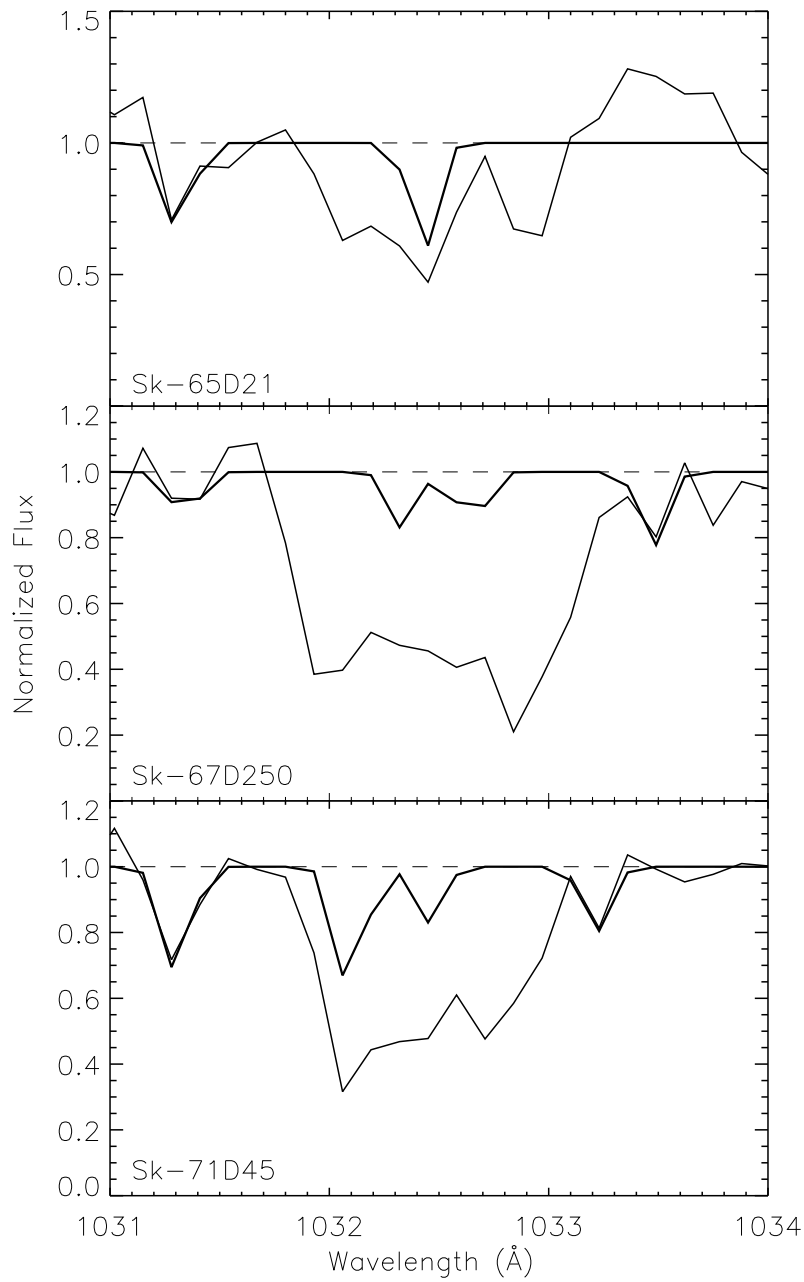


Figure 4. Model for H_2 absorption overplotted on the normalized O VI absorption profiles for 3 lines of sight. For Sk-65D21, H_2 absorption does not contaminate the LMC O VI absorption, while Sk-71D45 shows the maximum contamination. Sk-67D250 shows moderate contamination.

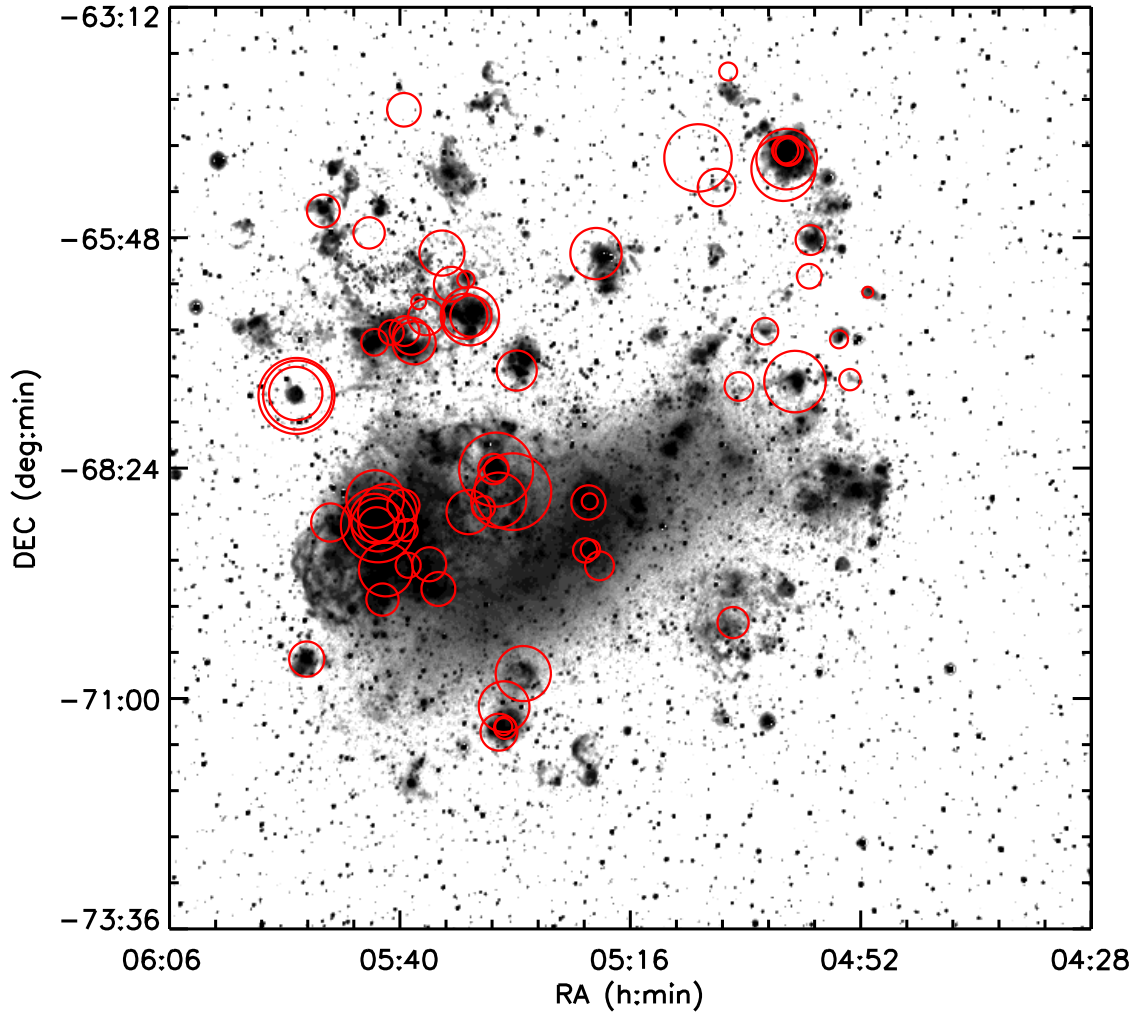


Figure 5. H_{α} image of the LMC (Gaustad et al. 2001) with circles showing O VI absorption around the 70 targets. The diameter of the circle is linearly proportional to the column density of O VI at LMC velocities.

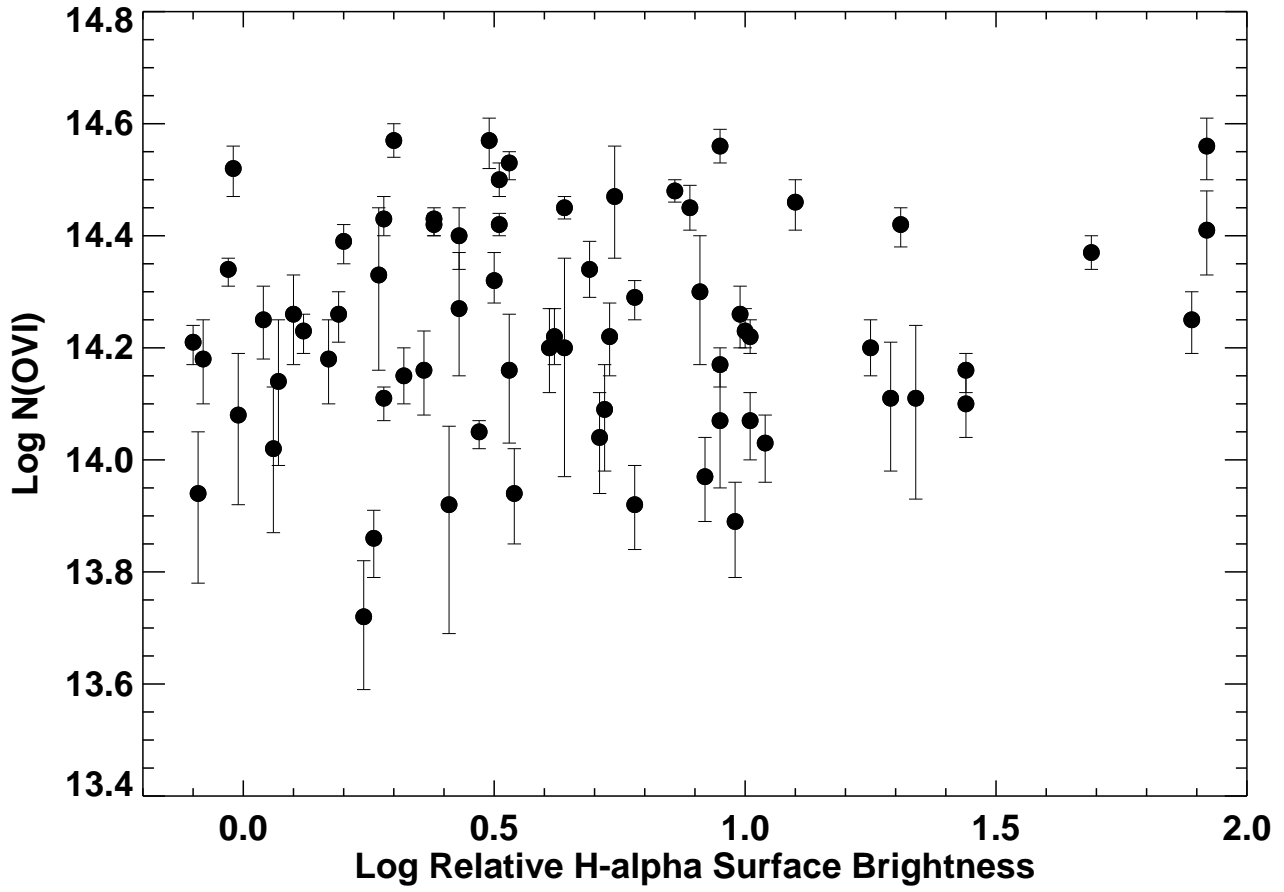


Figure 6. O VI column density ($\log N(\text{O VI})$) vs. \log relative H_α surface brightness for all the 70 targets. H_α surface brightness is from Gaustad et al. (2001).

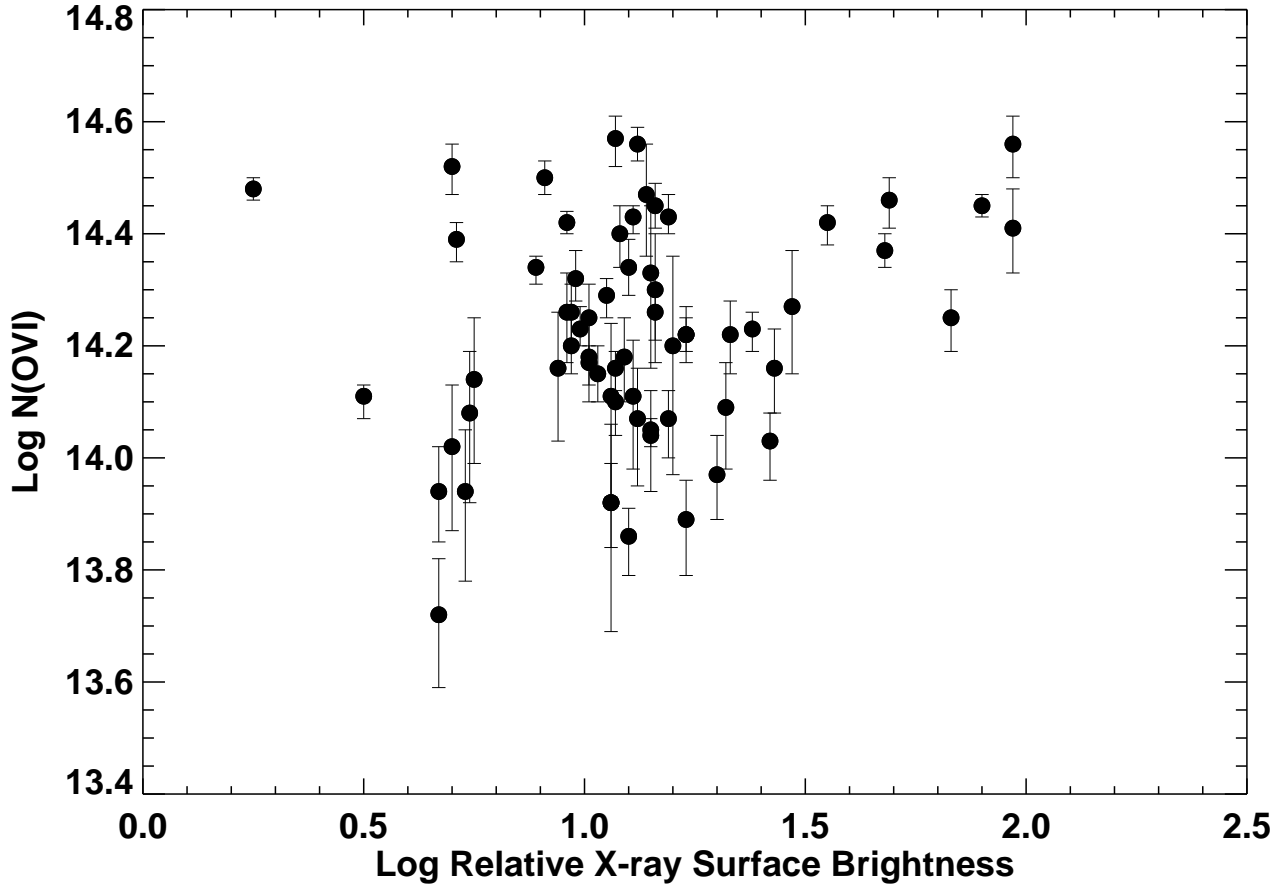


Figure 7. O VI column density ($\log N(\text{O VI})$) vs. log relative X-ray surface brightness for 65 targets. The X-ray surface brightness is taken from the *ROSAT* PSPC mosaic image (energy range 0.5–2.0 keV) (Snowden & Petre 1994). 4 targets (Sk-67D250, D301-1005, D301-NW8 and Sk-65D63) have not been covered by X-ray observations and one of the target Sk-69D257 has been excluded because it has extremely high X-ray emission.

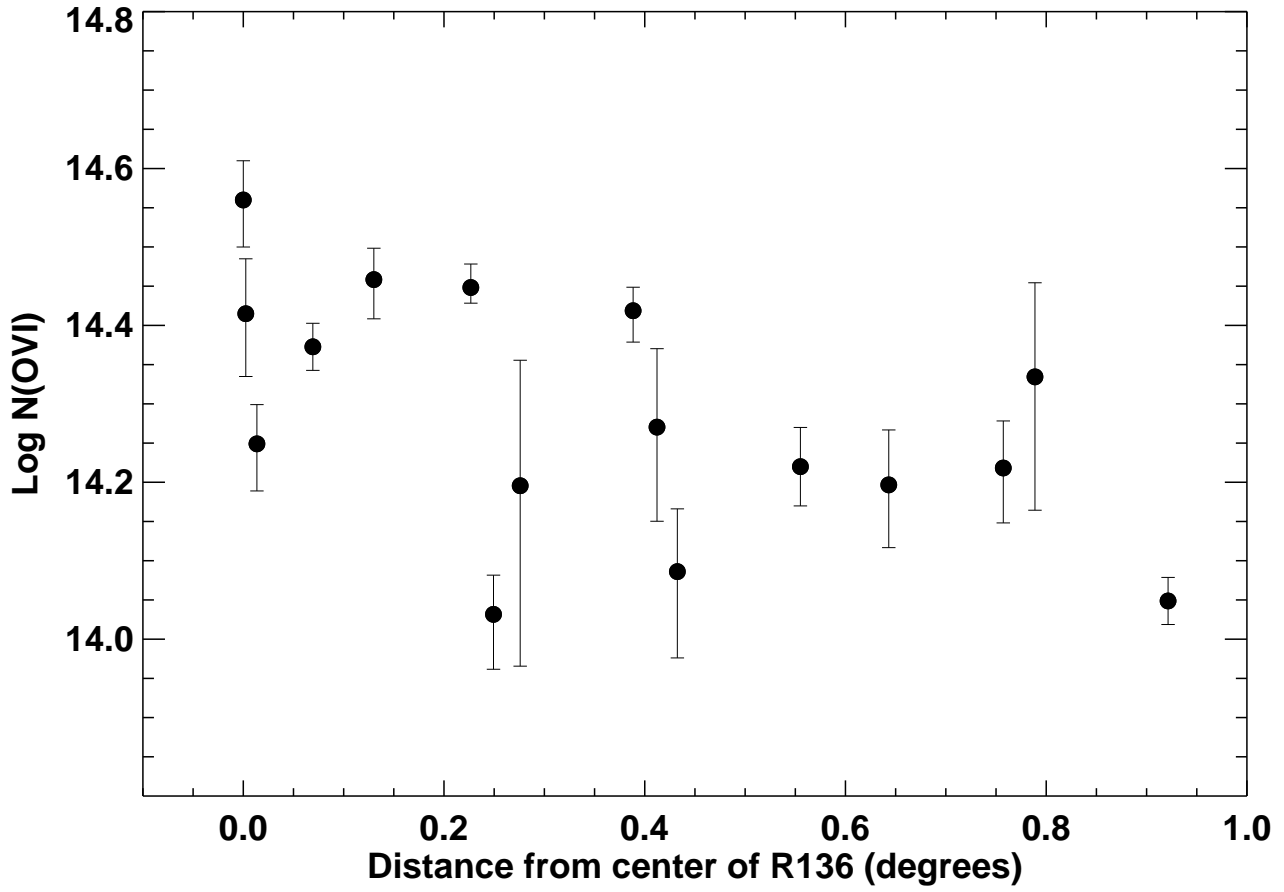


Figure 8. Variation of O VI column density ($\log N(\text{O VI})$) with increasing distance from the the centre of the star cluster R136 located in the 30 Doradus region of the LMC. Note that the variation is plotted within an angular distance of 1 degree from the the centre of R136.

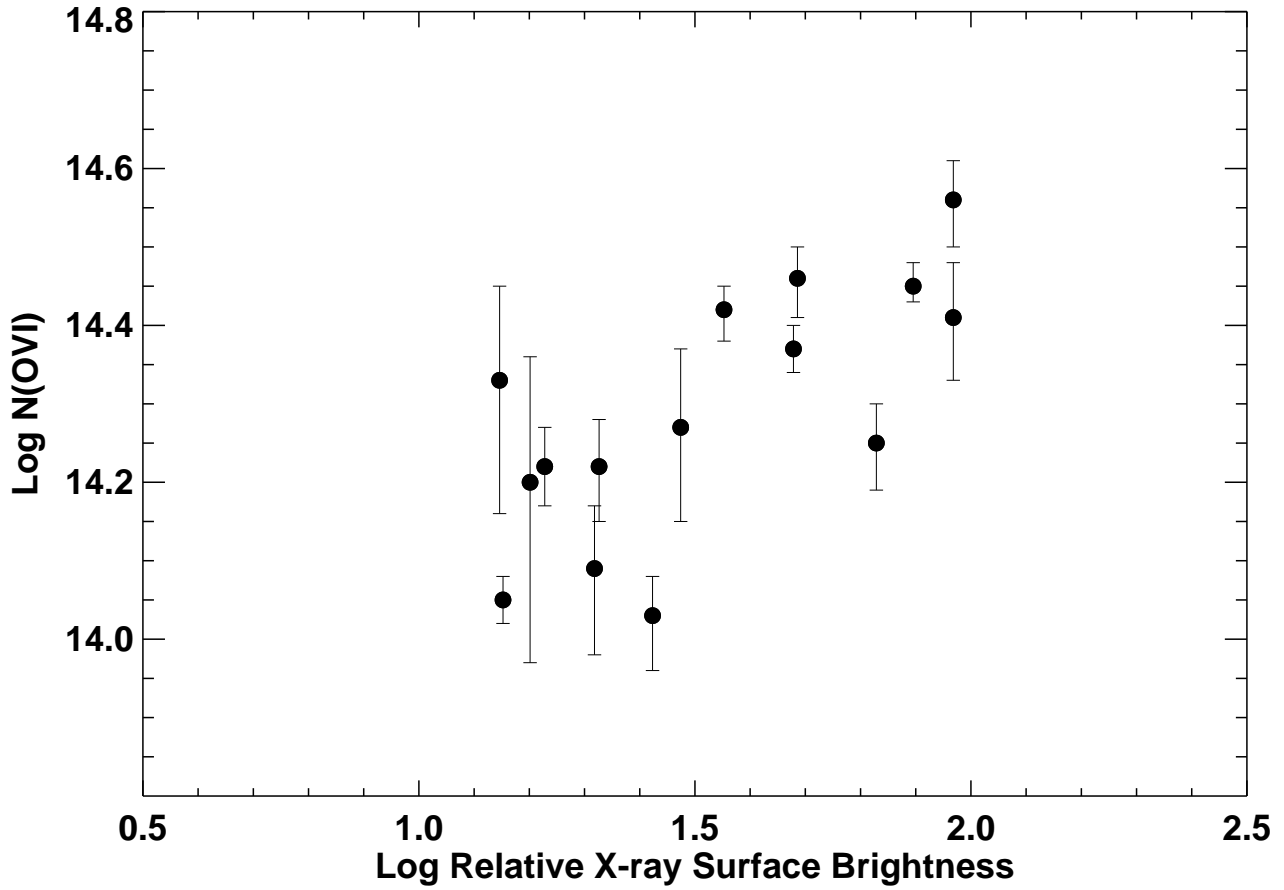


Figure 9. O VI column density ($\log N(\text{O VI})$) vs. X-ray luminosity for the 30 Doradus region of the LMC. The X-ray surface brightness is taken from the *ROSAT* PSPC mosaic image (energy range 0.5–2.0 keV) (Snowden & Petre 1994). A linear correlation is present which is not seen when all the targets of LMC are included (Fig. 7) and for other individual regions in the LMC. The plot includes all lines of sight from Fig. 8 except for 1 sightline (SK-69D257) as it shows an exceptionally high X-ray emission due to its proximity to X-ray binary LMC-X1 (Points et al. 2001).

Table 1: Log of *FUSE* observations for the 70 targets in the LMC.

<i>FUSE</i> ID	Object name	<i>FUSE</i> aperture	RA	Dec	Spectral Type	V mag.	Reference
P1030703	Sk-67D05	LWRS	04 50 18.96	-67 39 37.9	O9.7Ib	11.34	1
A0490402	Sk-68D03	LWRS	04 52 15.56	-68 24 26.9	O9I	13.13	2
E5111901	BI13	LWRS	04 53 06.48	-68 03 23.1	O6.5V	13.75	3
D0980801	Sk-67D18	MDRS	04 55 14.90	-67 11 24.5	O6-7n-nm+WN5-6A	11.95	1
P1174401	Sk-67D20	LWRS	04 55 31.50	-67 30 01.0	WN4b	13.86	4
B0100201	PGMW-3070	MDRS	04 56 43.25	-66 25 02.0	O6V	12.75	5
D0300302	LH103102	MDRS	04 56 45.40	-66 24 45.9	O7Vz	13.55	5
D0300101	LH91486	MDRS	04 56 55.58	-66 28 58.0	O6.5Vz	14.2	5
B0100701	PGMW-3223	MDRS	04 57 00.80	-66 24 25.3	O8.5IV	12.95	5
F9270604	HV2241	LWRS	04 57 15.83	-66 33 54.8	O7-III	13.5	5
P1174901	HD32402	LWRS	04 57 24.19	-68 23 57.2	WC		3
Z9050801	Sk-67D32	LWRS	04 59 52.30	-67 56 55.0	WN	14.48	3
P1030901	Sk-65D21	LWRS	05 01 22.33	-65 41 48.1	O9.7Iab	12.02	6
B0770201	HV2274	LWRS	05 02 40.96	-68 24 21.3	B0-B2III-I	14.2	5
P1174501	Sk-66D51	LWRS	05 03 10.20	-66 40 54.0	WN8h	12.71	4
D1380201	NGC1818-D1	LWRS	05 04 32.56	-66 24 51.0	B0-B2V-IV	14.93	5
P1172101	Sk-70D69	LWRS	05 05 18.73	-70 25 49.8	O5V	13.94	6
P1171703	Sk-67D69	LWRS	05 14 20.16	-67 08 03.5	O4III(f)	13.09	7
C1030101	MACHO78-6097	LWRS	05 18 04.70	-69 48 19.0	B0-B2V-IV	14.4	5
E5112902	BI130	LWRS	05 18 06.06	-69 14 34.5	O8.5V((f))	12.53	3
Z9050201	Sk-69D94	LWRS	05 18 14.53	-69 15 01.0	B0-B2III-I	9.72	5
D9044701	SNR0519-697	LWRS	05 18 44.20	-69 39 12.4	Supernova-remnant		
D0880104	BREY22	MDRS	05 19 16.40	-69 39 19.5	WC/O9.5Ib	12.3	1
B0270101	HD269445	LWRS	05 22 59.87	-68 01 46.6	WN	11.45	1
P1173602	Sk-69D124	LWRS	05 25 18.37	-69 03 11.1	O9Ib	12.81	2
D1530104	Sk-67D105	LWRS	05 26 06.37	-67 10 57.6	Of	12.42	5
A1110101	Sk-67D106	MDRS	05 26 15.20	-67 29 58.3	B0-B2III-I	11.78	8
A1110201	Sk-67D107	MDRS	05 26 20.67	-67 29 55.4	B0-B2III-I	12.5	8
C1510101	HD36521	LWRS	05 26 30.32	-68 50 25.4	WC	12.42	9
P1031402	Sk-68D80	LWRS	05 26 30.43	-68 50 26.6	WC4+OB	12.40	10
P2030104	Sk-68D82	LWRS	05 26 45.31	-68 49 52.8	WN5?b+(B3I)	9.86	5
P1173701	BI170	LWRS	05 26 47.79	-69 06 11.7	O9.5Ib	13.09	11
C1550201	Sk-67D111	LWRS	05 26 47.95	-67 29 29.9	O6:Iafpe	12.57	11
F9270701	HV2543	LWRS	05 27 27.40	-67 11 55.4	O8+O9	12.92	5
P1172501	Sk-70D91	LWRS	05 27 33.74	-70 36 48.3	O6.5V	12.78	11
P1172303	Sk-66D100	LWRS	05 27 45.59	-66 55 15.0	O6II(f)	13.26	6
E9570301	HDE269599	LWRS	05 28 22.68	-69 08 32.2	Be	10.18	5
M1142001	Sk-65D63	LWRS	05 28 39.50	-65 39 01.1	O9.7I	12.56	12
C1030201	HV982	LWRS	05 29 52.50	-69 09 22.0	B0-B2V-IV	14.6	5
E5113602	Sk-70D97	LWRS	05 30 11.35	-70 51 42.2	O9III	13.33	5
P1175001	Sk-67D144	LWRS	05 30 12.22	-67 26 08.4	WC4+OB	13.6	13
P2170301	BI184	LWRS	05 30 30.60	-71 02 31.3	B0-B2V-IV	13.84	3
D1380301	NGC2004-B15	MDRS	05 30 36.58	-67 17 42.3	B0-B2V-IV	14.18	5
Z9050601	Sk-71D38	LWRS	05 30 38.77	-71 01 47.9	WC	13.1	5
P1031502	Sk-71D45	LWRS	05 31 15.55	-71 04 08.9	O4-5III(f)	11.51	1
A1330123	Sk-67D166	LWRS	05 31 44.31	-67 38 00.6	O4If+	12.27	1
B0860901	Sk-67D168	MDRS	05 31 52.10	-67 34 20.8	O8Iaf	12.08	12
D9042002	SNR0532-675	LWRS	05 32 23.00	-67 31 02.0	Supernova-remnant		
P1173101	Sk-67D191	LWRS	05 33 34.12	-67 30 19.6	O8V	13.46	2
B0770302	HV5936	LWRS	05 33 39.00	-66 37 39.8	B0-B2V-IV	14.8	5
P1175101	Sk-69D191	LWRS	05 34 19.39	-69 45 10.0	WC4	13.35	13
F3210301	J053441-693139	LWRS	05 34 41.30	-69 31 39.0	O2-O3.5If*	13.7	14
P1171603	Sk-67D211	LWRS	05 35 13.92	-67 33 27.0	O2III(f)*	12.28	14
Z9051001	BREY64	LWRS	05 35 54.45	-68 59 07.4	WN9h	13.21	3
D9043101	SNR0536-692	LWRS	05 36 07.70	-69 11 52.6	Supernova-remnant		
Z9050701	Sk-69D220	LWRS	05 36 43.83	-69 29 47.4	WNorOiafpe	10.58	1
P1172201	Sk-66D172	LWRS	05 37 05.56	-66 21 35.7	O2III(f)*+OB	13.13	14
C0020601	BI253	LWRS	05 37 34.49	-69 01 09.8	Of	13.76	3
E5114201	Sk-68D137	LWRS	05 38 24.77	-68 52 32.8	O3III(f)	13.29	3
P1171803	MK42	LWRS	05 38 42.10	-69 05 54.7	O3If/WN6-A	10.96	15
P1031706	Sk-69D243	LWRS	05 38 42.57	-69 06 03.2	WN5+OB	9.5	16
F9140101	30DOR-S-R136	LWRS	05 38 51.70	-69 06 00.0	HII-region		
P1031802	Sk-69D246	LWRS	05 38 53.50	-69 02 00.7	WN	11.16	4
P1174601	HDE269927	LWRS	05 38 58.25	-69 29 19.1	WN	12.63	4
P2170101	Sk-69D257	LWRS	05 39 58.91	-69 44 03.2	O9II	12.53	5
D9042801	SNR0543-689	LWRS	05 43 07.20	-68 58 52.0	Supernova-remnant		
D0981401	D301-1005	MDRS	05 43 08.30	-67 50 52.4	O9.5V	14.11	3
D0981201	Sk-67D250	MDRS	05 43 15.48	-67 51 09.6	O7.5II(f)	12.68	17
D0981501	D301-NW8	MDRS	05 43 15.96	-67 49 51.0	D301-NW8	14.37	3
I8120701	Sk-70D115	LWRS	05 48 49.76	-70 03 57.5	O6.5Iaf	12.24	5

Notes. Units of right ascension are hours, minutes, and seconds; units of declination are in degrees, arcminutes, and arcseconds.

References – (1) Walborn (1977); (2) Conti et al. (1986); (3) Massey (2002); (4) Smith et al. (1996); (5) Blair et al. (2009); (6) Walborn et al. (1995); (7) Garmany & Walborn (1987) (8) Rousseau et al. (1978); (9) Moffat et al. (1990); (10) Smith et al. (1990); (11) Walborn et al. (2002b) (12) Fitzpatrick et al. (1988); (13) Torres-Dodgen & Massey (1988); (14) Walborn et al. (2002a); (15) Walborn & Blades (1997); (16) Massey & Hunter (1998); (17) Massey et al. (1995)

Table 2: Equivalent widths and column densities with corresponding velocity limits for O VI absorption in the LMC.

Target name	Equivalent width (mÅ)	log N(O VI) (dex)	Integration limits (km s ⁻¹)
Sk-67D05	73±6	13.72 ^{+0.10} _{-0.13}	175, 330
Sk-68D03	112±8	14.02 ^{+0.11} _{-0.15}	180, 330
BI13	88±4	13.94 ^{+0.08} _{-0.09}	175, 315
Sk-67D18	132±7	14.16 ^{+0.09} _{-0.13}	165, 330
Sk-67D20	147±8	14.08 ^{+0.11} _{-0.16}	175, 335
PGMW-3070	132±23	14.10 ^{+0.13} _{-0.18}	180, 345
LH103102	132±23	14.16 ^{+0.03} _{-0.04}	180, 330
LH91486	266±29	14.47 ^{+0.09} _{-0.11}	175, 385
PGMW-3223	129±15	14.10 ^{+0.06} _{-0.07}	175, 315
HV2241	271±18	14.50 ^{+0.04} _{-0.03}	165, 365
HD32402	271±8	14.48 ^{+0.02} _{-0.02}	160, 320
Sk-67D32	129±7	14.11 ^{+0.03} _{-0.04}	165, 360
Sk-65D21	94±23	13.94 ^{+0.11} _{-0.16}	225, 340
HV2274	160±11	14.14 ^{+0.10} _{-0.15}	165, 345
Sk-66D51	185±10	14.26 ^{+0.07} _{-0.09}	170, 370
NGC1818-D1	280±13	14.52 ^{+0.05} _{-0.05}	150, 340
Sk-70D69	182±12	14.18 ^{+0.07} _{-0.08}	150, 295
Sk-67D69	232±28	14.40 ^{+0.05} _{-0.06}	170, 340
MACHO78-6097	151±25	14.15 ^{+0.05} _{-0.05}	165, 320
BI130	94±7	13.89 ^{+0.07} _{-0.09}	165, 320
Sk-69D94	150±3	14.22 ^{+0.03} _{-0.03}	160, 340
SNR0519-697	97±4	13.97 ^{+0.07} _{-0.08}	160, 300
BREY22	126±24	14.07 ^{+0.06} _{-0.07}	160, 330
HD269445	200±10	14.29 ^{+0.04} _{-0.05}	175, 365
Sk-69D124	331±8	14.57 ^{+0.04} _{-0.05}	190, 430
Sk-67D105	110±8	13.92 ^{+0.14} _{-0.23}	180, 320
Sk-67D106	180±7	14.30 ^{+0.10} _{-0.13}	175, 345
Sk-67D107	254±10	14.45 ^{+0.04} _{-0.05}	160, 360
HD36521	126±9	14.07 ^{+0.09} _{-0.12}	175, 340
Sk-68D80	303±16	14.56 ^{+0.04} _{-0.03}	145, 335
Sk-68D82	141±10	14.17 ^{+0.04} _{-0.04}	165, 320
BI170	235±20	14.43 ^{+0.02} _{-0.03}	165, 365
Sk-67D111	214±19	14.34 ^{+0.05} _{-0.05}	175, 365
HV2543	156±42	14.23 ^{+0.04} _{-0.03}	160, 365
Sk-70D91	256±7	14.43 ^{+0.04} _{-0.03}	160, 365
Sk-66D100	214±21	14.34 ^{+0.03} _{-0.03}	160, 340
HDE269599	123±6	14.05 ^{+0.03} _{-0.03}	165, 320
Sk-65D63	184±8	14.21 ^{+0.04} _{-0.04}	180, 375
HV982	208±58	14.33 ^{+0.12} _{-0.17}	175, 360
Sk-70D97	226±4	14.39 ^{+0.03} _{-0.04}	175, 375
Sk-67D144	194±10	14.25 ^{+0.06} _{-0.07}	165, 335
BI184	118±10	14.04 ^{+0.08} _{-0.10}	165, 330
NGC2004-B15	92±7	13.86 ^{+0.05} _{-0.07}	175, 330
Sk-71D38	94±7	13.92 ^{+0.07} _{-0.08}	165, 315
Sk-71D45	194±9	14.26 ^{+0.06} _{-0.06}	160, 345
Sk-67D166	206±9	14.32 ^{+0.05} _{-0.05}	165, 390
Sk-67D168	186±12	14.26 ^{+0.05} _{-0.05}	165, 375
SNR0532-675	147±9	14.16 ^{+0.07} _{-0.08}	165, 345
Sk-67D191	229±16	14.42 ^{+0.02} _{-0.02}	165, 340
HV5936	174±8	14.18 ^{+0.07} _{-0.08}	175, 375
Sk-69D191	185±25	14.22 ^{+0.06} _{-0.07}	165, 340
J053441-693139	182±33	14.22 ^{+0.05} _{-0.05}	165, 330
Sk-67D211	144±8	14.11 ^{+0.10} _{-0.13}	160, 350
BREY64	139±8	14.20 ^{+0.16} _{-0.23}	180, 330
SNR0536-692	116±7	14.03 ^{+0.05} _{-0.07}	165, 320
Sk-69D220	128±9	14.09 ^{+0.08} _{-0.11}	160, 315
Sk-66D172	173±9	14.20 ^{+0.05} _{-0.05}	175, 360
BI253	259±46	14.46 ^{+0.04} _{-0.05}	160, 300
Sk-68D137	234±7	14.45 ^{+0.03} _{-0.02}	165, 330
MK42	228±24	14.41 ^{+0.07} _{-0.08}	160, 330
Sk-69D243	307±15	14.56 ^{+0.05} _{-0.06}	150, 345
30DOR-S-R136	185±25	14.25 ^{+0.05} _{-0.06}	165, 320
Sk-69D246	211±7	14.37 ^{+0.03} _{-0.03}	155, 325

Continued on Next Page...

Table 2 – Continued

Target name	Equivalent width (mÅ)	log N(O VI) (dex)	Integration limits (km s ⁻¹)
HDE269927	245±8	14.42 ^{+0.03} _{-0.04}	160, 320
Sk-69D257	171±8	14.20 ^{+0.07} _{-0.08}	160, 315
SNR0543-689	186±34	14.27 ^{+0.10} _{-0.12}	160, 360
D301-1005	284±57	14.53 ^{+0.02} _{-0.03}	165, 385
Sk-67D250	316±33	14.57 ^{+0.03} _{-0.03}	165, 375
D301-NW8	228±30	14.42 ^{+0.02} _{-0.03}	175, 365
Sk-70D115	186±11	14.23 ^{+0.03} _{-0.04}	165, 330

Notes. The errors in equivalent widths and column densities are 1σ error estimates. Integration limits gives the velocity range over which the LMC O VI absorption profile was integrated.

Table 3. O VI column densities in the superbubbles (SB) of the LMC.

Target name	Superbubble	Column density (10^{14} atoms cm^{-2})	$\log N(\text{O VI})$ (dex)
Sk-69D246	30Dor C	$2.36^{+0.18}_{-0.14}$	$14.37^{+0.03}_{-0.03}$
MK42	30Dor C	$2.60^{+0.46}_{-0.45}$	$14.41^{+0.07}_{-0.08}$
30DOR-S-R136	30Dor C	$1.77^{+0.20}_{-0.24}$	$14.25^{+0.05}_{-0.06}$
Sk-69D243	30Dor C	$3.63^{+0.40}_{-0.45}$	$14.56^{+0.05}_{-0.06}$
Sk-69D191	N154	$1.65^{+0.26}_{-0.23}$	$14.22^{+0.06}_{-0.07}$
HDE269927	N158	$2.62^{+0.16}_{-0.21}$	$14.42^{+0.03}_{-0.04}$
Sk-68D80	N144	$3.61^{+0.30}_{-0.26}$	$14.56^{+0.03}_{-0.03}$
HD36521	N144	$1.18^{+0.28}_{-0.28}$	$14.07^{+0.09}_{-0.11}$
BI184	N206	$1.09^{+0.22}_{-0.22}$	$14.04^{+0.08}_{-0.10}$
Sk-71D45	N206	$1.80^{+0.24}_{-0.21}$	$14.26^{+0.06}_{-0.06}$
Sk-70D91	N204	$2.69^{+0.24}_{-0.17}$	$14.43^{+0.04}_{-0.03}$
PGMW-3223	N11	$1.27^{+0.18}_{-0.18}$	$14.10^{+0.06}_{-0.07}$
LH103102	N11	$1.46^{+0.10}_{-0.13}$	$14.16^{+0.03}_{-0.04}$
PGMW-3070	N11	$1.27^{+0.43}_{-0.43}$	$14.10^{+0.13}_{-0.18}$
LH91486	N11	$2.96^{+0.68}_{-0.68}$	$14.47^{+0.09}_{-0.11}$
Sk-67D111	N51	$2.20^{+0.29}_{-0.24}$	$14.34^{+0.05}_{-0.05}$
Sk-67D107	N51	$2.85^{+0.27}_{-0.27}$	$14.45^{+0.04}_{-0.05}$
Sk-67D106	N51	$2.01^{+0.50}_{-0.53}$	$14.30^{+0.10}_{-0.13}$
Sk-67D166	N57	$2.09^{+0.25}_{-0.20}$	$14.32^{+0.05}_{-0.05}$
Sk-67D250	N70	$3.71^{+0.23}_{-0.23}$	$14.57^{+0.03}_{-0.03}$
D301-1005	N70	$3.37^{+0.17}_{-0.22}$	$14.53^{+0.02}_{-0.03}$
D301-NW8	N70	$2.60^{+0.09}_{-0.13}$	$14.42^{+0.02}_{-0.03}$
Total SB (this work)		2.31 ± 0.12	14.35 ± 0.18
Total non-SB (this work)		1.68 ± 0.12	14.19 ± 0.23
Total SB N70 ¹		3.04 ± 0.45	14.48 ± 0.06
Total non-SB ¹		2.03 ± 0.58	14.29 ± 0.14
Total SB ²		3.07 ± 0.62	14.48 ± 0.09
Total non-SB ²		2.10 ± 0.50	14.31 ± 0.11

Notes. The superbubble lines of sight are shown in Fig. 1.

(1) Danforth & Blair (2006); (2) Combined data of Howk et al. (2002a) and Danforth & Blair (2006).